# MULTIPLE ADIABATIC BEDS FOR EFFICIENT CONVERSION OF $CO_2$-CONTAINING SYNGAS TO DIMETHYL ETHER

by

Ceren Hatipoğlu

B.S., Chemical Engineering, Boğaziçi University, 2019

Submitted to the Institute for Graduate Studies in
Science and Engineering in partial fulfillment of
the requirements for the degree of
Master of Science

Graduate Program in Chemical Engineering

Boğaziçi University

2021

# ACKNOWLEDGEMENTS

I would like to express my deepest appreciation to my supervisor Prof. Ahmet Kerim Avcı, who holds a profound belief in my work with a great understanding and patience. I wish to thank him for his convincing guidance, giving me a lot of encouragement to accomplish my research. Also, he became more of a supportive mentor, than a professor especially when I lost my auntie during the COVID-19 pandemic. Without his persistent professional help, I would not be able to reach to the tip of the mountain covered with obstacles.

Besides, I owe a lot to Assoc. Prof. Kerem Uğuz, Prof. Ramazan Yıldırım and Assoc. Prof. Burak Alakent for their academic and insightful personal guidances.

I would like to extend my sincere thanks to my friends in KB-404, Necdet Semih Altınsoy, Hasan Köybaşı, Mert Özden, Nusret Furkan Öztürk, Özge Selçuk, Uğurcan Tozar. I am also so grateful to my friends who shared their valuable time with me in KB with joy; Selma Başıbüyük, Onur Boy, Özge Duman, Pınar Eribol, Burakhan Ertürk, Elif Esvap, Seymen İlke Kaykanat, İlkay İrem Özbek, Pınar Özdemir, Mustafa Sertbaş, Enes Emre Taş, Selin Taşkın. I owe them special thanks for helping me when I was struggling with an issue and encouraging me when I was worried about my research.

Of course, I must thank my family for being always by my side during my road map. I am greatly indebted to my parents and my elder-sister Canan for their unwavering support. Also, I very much appreciate my closest friends, Deniz Güngöroğlu, Ecem Naz Vanlı and Irmak Ünal, who make me feel always behind me..

This study was supported by Bogazici University Research Fund (Grant number: BAP-16463) and by TUBITAK (Grant number: 118M518).

To my sweet auntie, Fatma: Rest in peace; may the eternal serenity find you..

# ABSTRACT

## MULTIPLE ADIABATIC BEDS FOR EFFICIENT CONVERSION OF $CO_2$-CONTAINING SYNGAS TO DIMETHYL ETHER

DME is considered for replacing its conventional counterparts due to its attractive properties such as CO+$NO_x$ free combustion characteristics. DME production involves exothermic equilibrium reactions, namely synthesis gas-to-methanol conversion and subsequent dehydration of methanol, necessitating the use of synthesis and solid acid catalysts, respectively. The co-existence of catalysts in the same reactor is called direct DME synthesis, which is limited by thermodynamic effects induced by increased temperatures and $H_2O$ generated during the process. A novel reactor strategy to overcome thermodynamic constraints is the so-called multiple adiabatic beds which involve adiabatic packed-bed reactors interconnected with microchannel heat exchangers. The microchannel heat-exchangers, selected for their inherently high heat transfer rates and compact characteristics, are used to decrease temperature for the successive beds. When equipped with a steam-selective membrane, the heat-exchangers also used to remove $H_2O$ from the reactive mixture. Reactors include 1:1 (by mass) physical mixtures of to each bed CZA+$\gamma$-$Al_2O_3$, or CZA+HZSM-5 catalysts. Packed-bed reactors are simulated by the steady-state 1D pseudo-homogeneous reactor model involving literature-based reaction kinetics. Modeling of the microchannel heat-exchangers, however, are carried out by solution of the Navier-Stokes equations along with heat transport at 2D steady-state under ANSYS platform. The effects of inlet temperature, pressure and the amount of catalyst are studied in the range of 493-513 K, 20-60 bar and 0.15-0.18 kg catalyst respectively. The results show that the proposed reactor strategy offers the potential of relaxing the characteristic thermodynamic constraints of one-step DME synthesis.

# ÖZET

## ÇOKLU YATAKLI ADİYABATİK REAKTÖRLER İLE $CO_2$ İÇERİKLİ SENTEZ GAZININ DİMETİL ETERE VERİMLİ DÖNÜŞÜMÜ

DME, CO ve $NO_x$ salımı olmaksızın yanabilme gibi çekici özellikleriyle geleneksel yakıtların yerini alabileceği düşünülmektedir. DME üretimi, sırasıyla sentez ve katı asit katalizörleri kullanılarak, sentez gazının metanole dönüşümü ve ardından metanolün dehidrasyonu ekzotermik denge tepkimelerini içerir. Katalizörlerin aynı reaktörde bir arada bulunmasını içeren süreç doğrudan (tek aşamalı) DME sentezi olarak tanımlanıp, bu süreç artan sıcaklıklar ve işlem sırasında üretilen $H_2O$ tarafından teşvik edilen ters termodinamik etkilerle sınırlıdır. Termodinamik kısıtları aşabilmek için önerilen yenilikçi bir reaktör stratejisi olan çoklu adiyabatik yatak yapısı, birbirlerine mikrokanallı ısı değiştiricilerle bağlı, adiyabatik koşullarda çalışan dolgu yataklı reaktörlerden oluşmaktadır. Karakteristik olarak yüksek ısı iletim hızlarına ve kompakt yapıya sahip mikro kanallı ısı eşanjörleri, ardışık yataklarda yükselen sıcaklığı düşürmek için kullanılmaktadır. Mikro kanallı ısı eşanjörleri su buharı seçici bir membran ile donatıldığında soğutmaya ek olarak reaktif karışımdan suyu çekmek için de kullanılabilmektedir. Her yatak, CZA+$\gamma$-$Al_2O_3$ veya CZA+HZSM-5 katalizörlerinin 1:1 (kütlece) fiziksel karışımlarını içerir. Dolgu yataklı reaktörler, literatüre dayalı reaksiyon kinetiğiyle kararlı durum koşullarında tek boyutlu psödo homojen reaktör modeli kullanılarak tasarlanmıştır. Mikrokanallı ısı eşanjörlerinin modellenmesi, Navier-Stokes ve ısı iletimi denklemlerinin iki boyutta ANSYS platformunda çözümü ile yapılmıştır. Simulasyon çalışmaları, her yatağın giriş sıcaklığına, basıncına ve katalizör miktarına göre sırasıyla 493-513 K, 20-60 bar ve 0.15-0.18 kg katalizör aralığında elde edilmiştir. Sonuçlar, bu çalışmada önerilen reaktör stratejisinin tek aşamalı DME sentezinin karakteristik termodinamik kısıtlarını aşmaya yardımcı olabileceğini göstermektedir.

# TABLE OF CONTENTS

# LIST OF FIGURES

# LIST OF TABLES

# LIST OF SYMBOLS

| | |
|---|---|
| 0 | Initial condition |
| $A_c$ | Cross−sectonal area ($m^2$) |
| $c_{p,m}$ | Heat capacity of gas mixture ($J.kg^{-1}.K^{-1}$) |
| $D_{i,m}$ | Diffusion coefficient of species i in the mixture ($m^2.s^{-1}$) |
| $D_m$ | Diffusion coefficient of the mixture ($m^2.s^{-1}$) |
| $D_{in}$ | Inner diameter (m) |
| $D_p$ | Particle diameter (m) |
| $E_i$ | Overall energy of species $i$ (J) |
| F | Molar flow-rate ($mol.s^{-1}$) |
| $f_i$ | Fugacity of pure species $i$ (bar) |
| g | Gravitational acceleration ($m.s^{-2}$) |
| G | Superficial mass velocity (($\rho_m$.u),$kg.m.s^{-2}$) |
| $G_{f,i}$ | Gibbs free energy of formation of species $i$ ($kJ.mol^{-1}$) |
| $H_{f,i}$ | Enthapy of formation of species $i$ ($kJ.mol^{-1}$) |
| $\vec{I}$ | 3×3 Identity vector |
| $i$ | Species index |
| $\vec{J}_i$ | Diffusive mass flux of species i ($kg.s^{-1}.m^{-2}$) |
| $K_i$ | Adsorption constant of species $i$ ($bar^{-1}$) |
| $K_{rxn}$ | Equilibrium constant of reaction $MS_1$, $MS_2$, MD |
| $k_{rxn}$ | Reaction rate constant of $MS_1$, $MS_2$ and MD reactions |
| $k_m$ | Thermal conductivity of mixture ($W.m^{-1}.K^{-1}$) |
| $k_w$ | Thermal conductivity of wall separating the microchannels ($W.m^{-1}.K^{-1}$) |
| L | Length of the reactor (m) |
| $M_{A,i}$ | Molecular mass of species $i$ ($g.mol^{-1}$) |
| $m_{w.chip}$ | Wood consumption rate $i$ ($kg.wood\text{-}chip^{-1}$) |
| $n_i$ | Number of moles of species $i$ (mol) |
| $\vec{n}$ | Normal vector |
| $Q_{vol}$ | Volumetric flow rate ($m^3.s^{-1}$) |

| | |
|---|---|
| $\dot{Q}$ | Heat flow ($J.s^{-1}$) |
| P | Total Pressure (bar) |
| p | Particle |
| R | Gas constant (8.31447 $J.K^{-1}.mol^{-1}$) |
| $r_{rxn}$ | Rate of reaction $MS_1$, $MS_2$, MD, (mol.kg-$cat^{-1}.s^{-1}$) |
| $R_i$ | Consumption or generation rate of species $i$ (mol.kg-$cat^{-1}.s^{-1}$) |
| Re | Reynolds number |
| $S_{f,i}$ | Entropy of formation of species $i$ ($kJ.mol^{-1}.K^{-1}$) |
| t | Time ($s^{-1}$) |
| T | Temperature (K) |
| $T_c$ | Critical temperature (K) |
| $T_r$ | Residual temperature |
| $w_{cat}$ | Catalyst weight (kg) |
| W | Mechanical work (J) |
| $W_s$ | Shaft work (J) |
| u | Superficial velocity ($m.s^{-1}$) |
| $U_i$ | Internal energy of species $i$ (J) |
| $\vec{v}$ | Velocity vector ($m.s^{-1}$) |
| w | Weight of catalyst fed into the bed (kg) |
| x,y,z | Cartesian coordinates |
| $y_i$ | Mol fraction of species $i$ |
| $Y_i$ | Mass fraction of species $i$ |
| | |
| $\chi$ | Conversion (%) |
| $\delta$ | Dipole, (debye) |
| $\Delta G_{rxn}$ | Gibbs free energy of reaction ($MS_1$,$MS_2$,MD,$kJ.mol^{-1}$) |
| $\Delta H^0$ | Standard Enthalpy of reaction ($MS_1$,$MS_2$,MD, $kJ.mol^{-1}$) |
| $\Delta H_{rxn}$ | Enthalpies of reaction ($MS_1$,$MS_2$,MD,($kJ.mol^{-1}$) |
| $\epsilon$ | Porosity of the bed |
| $\mu_i$ | Viscosity of species i ($kg.m^{-1}s^{-1}$) |

| | |
|---|---|
| $\mu_m$ | Viscosity of the mixture ($\mathrm{kg.m^{-1}s^{-1}}$) |
| $\rho_b$ | Bulk density of the catalyst ($\mathrm{kg.m^{-3}}$) |
| $\rho_i$ | Density of species $i$ ($\mathrm{kg.m^{-3}}$) |
| $\rho_m$ | Density of the mixture ($\mathrm{kg.m^{-3}}$) |
| $\rho_w$ | Density of the wall ($\mathrm{kg.m^{-3}}$) |
| $\omega$ | Acentric factor |
| $\upsilon$ | Stoichiometric coefficient |

# LIST OF ACRONYMS/ABBREVIATIONS

| | |
|---|---|
| 1D | One dimensional |
| 2D | Two dimensional |
| 3D | Three Dimensional |
| $CH_3OH$ | Methyl alcohol (Methanol) |
| $CH_4$ | Methane |
| CO | Carbon monoxide |
| $CO_2$ | Carbon dioxide |
| Conf | Configuration |
| CZA | Copper-zinc oxide-alumina, catalyst for $MS_1$ and $MS_1$ reactions (Cu-ZnO/$Al_2O_3$) |
| $CH_3OCH_3$ | Dimethyl ether (DME) |
| FeCr | Iron chromium |
| $H_2$ | Hydrogen |
| $H_2O$ | Water in vapor phase |
| HEX | Heat-exchanger |
| HZSM-5 | Zeolite socony mobil no. 5, catalyst for MD reaction |
| LPG | Liquified petroleum gas |
| MD | Methanol dehydration |
| $MS_1$ | Methanol synthesis from carbon monoxide |
| $MS_2$ | Methanol synthesis from carbon dioxide |
| MW | Molecular weight |
| $N_2$ | Nitrogen |
| $NO_x$ | Nitrogen oxides |
| PBR | Packed-bed reactor |
| RWGS | Reverse water-gas shift reaction |
| S.steel | Stainless steel |
| WGS | Water-gas shift reaction |
| | |
| $\gamma$-$Al_2O_3$ | Catalyst for MD reaction |

# LIST OF SUBSCRIPTS/SUPERSCRIPTS

| | |
|---|---|
| $c$ | Critical |
| $cat$ | Catalyst |
| $f$ | Formation |
| $in$ | Inlet |
| $m$ | Mixture |
| $N$ | Normal condition |
| $out$ | Outlet |
| $r$ | Residual |
| $react$ | Reactor |
| $rxn$ | Reaction |
| $sw$ | Sweep gas |
| $syn$ | Syngas |

# 1. INTRODUCTION

$CO_2$ emission is a global phenomenon posing a serious threat to both environment and living species on earth. The dramatic increase in the release of greenhouse gases such as CO, $CO_2$, $CH_4$ into the atmosphere leads to one of the most pressing challenges, global warming. When devastating ecological, physical and health impacts on climate change investigated within decades, governments have begun to make regulations and budgets for reducing $CO_2$ concentrations in the atmosphere. In this respect, to mitigate the imminent consequences of global warming such as global temperature increase, sea-level rise and altered crop growth, the Intergovernmental Panel on Climate Change (IPCC) and the United Nations Climate Change Conference (COP21, Paris, 2015) decided that $CO_2$ emission be halved and the global average temperature rise should should be limited to 2 °C [1–3].

The main sources for $CO_2$ release should be regulated to minimize the effects of global warming. Petroleum refineries, petrochemical facilities, cement plants and especially coal-based power plants which are fed by fossil fuels to fulfil examples of industrial-scale causes for $CO_2$ release [3,4]. In daily life, on the other hand, the largest proportion for carbon emissions originates from internal combustion engine vehicles [5]. Transportation and residential needs, and agricultural activities such as rice production as well as agricultural soils comprise approximately 35 % of $CO_2$ emission as shown in the Figure 1.1 [6].

As mentioned in the previous paragraphs, fossil fuels, particularly coal and natural gas, are the main causes of $CO_2$ emission paving the way for renewable fuel resources as a favourable alternatives. Hence, bio-based fuels have been of common interest for both researchers and consumers in recent years. Moreover, biomass is not only sustainable and environmentally friendly, but it also acquires similarities with fossil fuels in terms of thermodynamics. By using biofuels such as ethanol and biodiesel, bioenergy can be obtained via gasification, reforming or combustion routes [7–9].

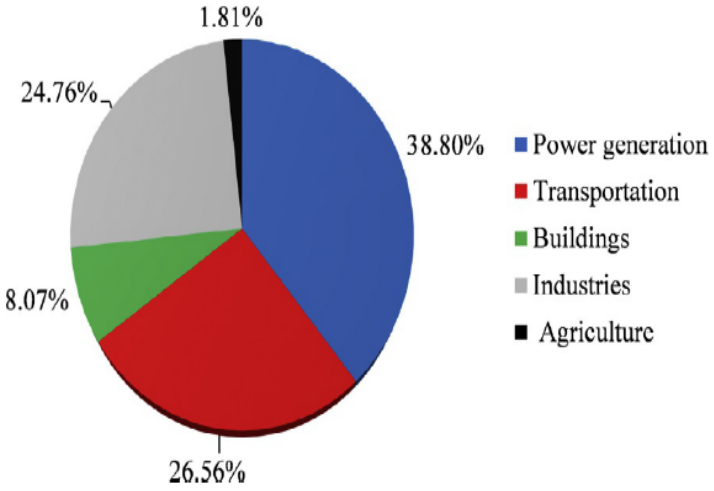


Figure 1.1. The global distribution of $CO_2$ emissions with respect to sectors in 2019 [6].

Among alternative energy fuels, dimethyl ether (DME) produced from syngas and methanol obtained from bio-based resources has become promising fuel [10]. DME is more favourable in terms of easy transportation and handling due to its low boiling point [10]. Moreover, its combustion accumulates lesser emissions of CO and NO [10]. Besides, combustion properties of DME are very similar to those of diesel. Hence with small adjustments, it can be used in the conventional diesel engines [11]. Also, when compared with LPG – a mixture of propane and butane – DME is relatively non-toxic as well as non-carcinogenic in domestic use [2, 11].

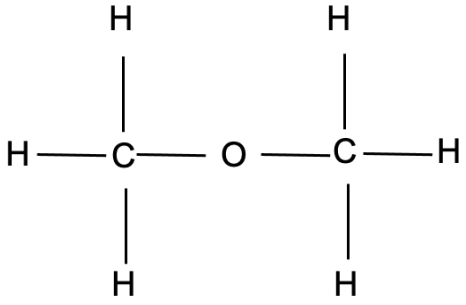


Figure 1.2. Molecular structure of dimethyl ether (DME).

With regard to chemical and physical properties, dimethyl ether is a highly volatile gas under normal conditions. A blue flame, which is also a specific combustion attribute of natural gas, glows when combusted with oxygen [12]. Dimethyl ether turns into the liquid phase when pressurized to 5 bar [12]. Besides, it acquires the lower boiling and auto-ignition points compared to diesel. DME predominates diesel in terms of cetane number, which enables easy ignition and, in turn, more complete combustion [2,11]. In doing so, the fuel consumption and $CO_2$ emission decrease significantly. However, diesel almost doubles DME when lower heating value is considered in fuel injection as tabulated in Table 1.1 [2, 11–13]. In addition to physical properties, from Figure 1.2 above, it can be seen that DME's molecular structure comprises C-O and C-H single bonds [2, 12]. In one DME molecule, there is approximately 35 and 52 % of C and O by mass respectively.

In the DME production process, the downstream of syngas stemming from petrochemical or biochemical industries are used as a feedstock to minimize both CO and $CO_2$ release to the atmosphere. The syngas formation occurs as a result of reforming and gasification processes from biomass; dry or steam reforming and partial oxidation reactions from higher hydrocarbons [14]. In general, DME can be produced via two methods, namely by the direct and indirect route. In the first method, both the methanol synthesis and DME formation reactions take place in a single reactor involving either a bifunctional catalysis or the physical mixture of the methanol synthesis and dehydration catalysts [10]. The catalyst loaded for the first reaction is Cu–ZnO whereas for the latter, either $\gamma$-$Al_2O_3$ or HZSM-5 is used to drive the methanol dehydration [15, 16]. In the indirect approach, on the other hand, methanol synthesis and dehydration reactions are carried out in dedicated reactors [17]. The operating conditions, temperature and pressure, for methanol synthesis vary between 473–573 K and 30–70 atm at $H_2$/CO ratios of 2–5 [18, 19].

Direct synthesis has more advantages than indirect synthesis in terms of process operation and design cost of the system [18–20]. When both methanol formation and dehydration reactions are carried out in a single reactor, methanol formation is thermodynamically favoured. Hence, a significant increase in both CO and $CO_2$ conversion

and DME yield can be obtained [20]. However, as the indirect route consists of two consecutive packed-beds, the outlet of the first packed-bed should be purified, and, in turn, set to the required temperature and pressure for the methanol dehydration. Eventually, all these steps increase results in additional operating and design costs [19]. It should be noted that carrying out the exothermic methanol synthesis and dehydration reactions in a single packed-bed reactor brings certain obstacles such as catalyst deactivation, coking and also, safety concerns [20]. For that reason, temperature control is paramount in the direct approach to obtain desirable DME yield and syngas conversion.

Table 1.1. Physical Properties of DME and Diesel [2, 13].

| | DME | Diesel |
|---|---|---|
| Molecular formula | $CH_3OCH_3$ | $C_{10}H_{20}$ to $C_{15}H_{28}$ |
| Molecular weight (g/mol) | 46.07 | – |
| Liquid density (kg/m$^3$) | 667 | 831 |
| Appearance | Colorless | Colorless or yellow |
| Melting point (K) | 132 | 243 to 255 |
| Boiling point (K) | 249 | 450 to 643 |
| Autoignition point (K) | 508 | 523 |
| Vapor pressure (at 25 K) (bar) | 5.3 | $< 0.1$ |
| Lower heating value (at 25 K) (MJ/kg) | 27.6 | 42.5 |

In this study, the direct DME synthesis process is simulated in the adiabatic packed-bed reactors interconnected with microchannel heat-exchangers. In the proposed configuration, exothermic synthesis and methanol dehydration reactions take place adiabatically in packed-bed reactors. Adiabatic temperature rise is then reduced within the subsequent heat-exchanger such that the thermodynamic limitations are relaxed for the reactor following the heat-exchanger unit. Packed-bed reactors possess certain attractive characteristics such as low cost and simplicity in manufacturing. Also, high conversions and yields can be achieved with effective regulation of temperature [20]. In this respect, microchannel heat-exchangers offering very high surface

area-to-volume ratios (ca. $10^4$ $m^2/m^3$), become ideal. The microchannel units provide the advantage of effective temperature control together with notable intensification [21,22]. In these units, cold sweep gas and hot reactor outlet flow in countercurrent mode [21, 23].

This presented research aims to investigate direct DME synthesis process performed in cascade reactor system for both Cu-ZnO/$Al_2O_3$-$\gamma$-$Al_2O_3$ and Cu-ZnO/$Al_2O_3$-HZSM-5 catalysts in the context of syngas conversion and DME yield. For this purpose, packed-bed reactors, involving physical mixtures of methanol synthesis (Cu/ZnO/$Al_2O_3$) and dehydration ($\gamma$+$Al_2O_3$ or HZSM-5) catalysts, and microchannel heat-exchangers are modeled. The resulting models are used to understand the impacts of several operating parameters such as temperature and pressure, amount and type of catalyst and the structural parameters of the heat-exchangers. Owing to the possibility of integrating steam-selective membranes to microchannel heat-exchangers, the extent of steam removal is also studied. Consequently, it is aimed to design a compact catalytic reactor & heat-exchanger system that can effectively relax the thermodynamic limitations inhibiting direct conversion of $CO_2$-containing syngas to DME.

This thesis consists of 5 chapters divided into sections and subsections in detail. Chapter 2 includes an up-to-date literature survey regarding the reactor and catalysts types involved in direct DME synthesis. The literature survey also involves a theoretical background on both packed-bed reactor and microchannel heat-exchangers. Chapter 3 describes the details of the cascade reactor configuration and the mathematical models. Chapter 4 involves the results of the parametric studies and their discussions. Finally, major conclusions and some recommendations for future studies are described in Chapter 5.

# 2. LITERATURE SURVEY

## 2.1. Cascade Reactor System

Process intensification for chemical processes has been a common interest for researchers for economic and safety concerns. Cascade reactor configuration includes a combination of a conventional packed-bed reactor and a microchannel heat-exchanger which promises a compact and efficient design in terms of syngas conversion and DME yield for this research. In the following subsections, the attributes of each equipment are described for the scope of this study. The schematic configuration of the cascade reactor system is illustrated in Figure 2.1.

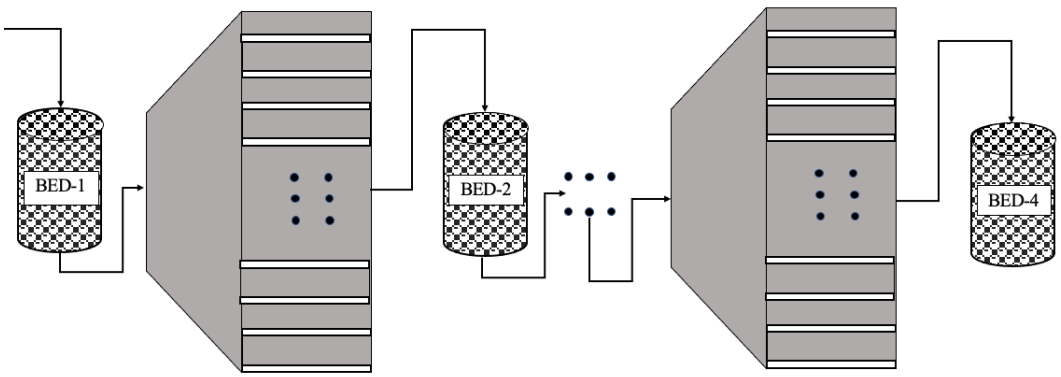


Figure 2.1. Cascade reactor configuration scheme [24] (drawing is not to scale).

The cascade reactor system consists of adiabatic packed-bed reactors connected by the microchannel heat-exchangers. The microchannels perform the required cooling of the reactor's outlet due to reactions' high exothermicity [25]. By splitting the catalytic beds into shorter packed-beds, when needed, catalyst replacement is achieved much easier without reactants replacement [25]. Furthermore, owing to the cooling provided either by cocurrent or countercurrent micro-scale heat-exchangers between each bed, much higher syngas conversion as well as DME yield values can be obtained [25,26].

The consecutive bed number can be adjusted to the limiting criteria such as pressure drop, specified conversion level, or maximum exit temperature [26]. The cascade reactor system is designed based on the classical approach of reactors followed by a separator providing interstage cooling/heating [25, 26]. The innovation of the former method comes with the replacement of the microchannel heat-exchanger for temperature regulation. In doing so, the cascade system's dimension becomes more compact and advantageous in terms of pressure drop [26]. The temperature limitations for DME synthesis make use of the cascade reactor system attractive in terms of the performance of catalysts and economical constraints.

### 2.1.1. Packed-Bed Reactors

Packed bed reactors have a wide range of use for catalytic reactions in both laboratory and industrial-scale owing to its simplicity and lower costs [27, 28]. The scheme of packed-bed reactor consists of a single bed in which catalyst is loaded either as a particle or powder form [29]. The packed-bed reactors possess certain beneficial attributes regarding the construction and maintenance of the fixed-bed reactor.

First of all, the application of packed-bed reactors in chemical industries is versatile. since the catalyst recover process is much easier compared to other configurations such as fluidized-bed or slurry reactors [28]. In addition, as the reactions take place in the fixed-bed along the reactor length, the contact time between the catalyst particles and inlet stream increases which, in turn, results in more conversion of the reactant and more formation of the product [11]. Due to more contact time, packed-bed reactors lead to higher conversion per weight of catalyst compared to other configurations [11,28,30].

The cylindrical shape of the packed-bed reactor is the most wide-known configuration rather than sphere due to practicality in catalyst recovery and plug flow assumption [12, 29]. In computational studies, the plug-flow assumption can be generally applicable in the packed-bed reactors meaning that the velocity of the fluid passing through the cross-section of the packed-bed remains constant along the reactor length [29]. This assumption can be satisfied with an aspect ratio greater than 5 [31].

In that way, the homogeneity of the physical and chemical properties of the reactant mixture does vary only with respect to the length of the reactor rather than radial direction [29, 31].

Despite substantial benefits, packed-bed reactors also have distinct disadvantages. The major problem in the packed-bed reactor is high-pressure drop along due to small catalyst particles in the bed [29]. The catalyst particles create significant resistance to the inlet passing through the reactor length, hence results in a considerable pressure drop. To combat this problem, either the reactor length is kept short, or the size of catalyst particles is enlarged in the design of the packed-bed. In both cases, the conversion of the reactant is limited due to physical constraints [32, 33].

Adiabatic beds provide an interesting optimum longitudinal profile of temperature from the inlet to the outlet of the reactor. For instance, if endothermic reactions are carried out in the PBR, the reaction rate is high near the inlet where conversion is far from that limited by thermodynamics [32]. By decreasing temperature along the reactor, the higher conversion is attained at the outlet where thermodynamic constraints take place [29]. On the other hand, when extremely exothermic reactions are carried out in the PBRs, temperature regulation becomes a big issue in the adiabatic packed-bed configuration. Hot spot generation results in catalyst sintering, thermodynamic limitation and undesirable methane formation in the DME synthesis process [19]. To mitigate its effect on the product, such as low selectivity and conversion, temperature control is paramount. If a proper temperature regulation is applied via heat utility equipment such as a heat-exchanger or a cooling channel around the reaction channel, the performance of the packed-bed reactor is enhanced sufficiently enough under high pressure and temperature [34]. In addition, high syngas recycle ratio is applied to maintain reactor at the optimum temperature. This strategy, however, causes lower per-pass conversions as well as larger capital investments and operating costs.

### 2.1.2. Microchannel Heat-Exchangers

The compactness of the heat-exchangers has become a striking challenge for numerous industries [35]. Microchannel heat-exchanger has become prominent among the others owing to its micro-scale dimensions with hydraulic diameter of 1-100 $\mu$m and the higher efficiency in the heat transfer [35]. The repeating unit of the microchannel heat-exchanger includes two parallel channels, which hot and cold fluid pass in either cocurrently or counter-currently, are separated with a thicker wall.

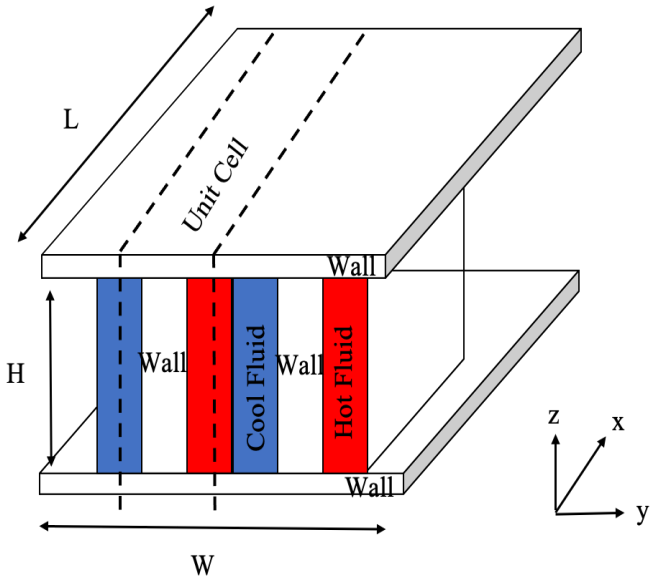


Figure 2.2. The microchannel heat-exchanger configuration (adapted from [36]) (drawing is not to scale).

Microchannel heat-exchanger offers a considerably high surface area to volume ratios up to ca. $10^4$ $m^2/m^3$ [37] which results in increased overall heat transfer coefficients ranging from 2600 $W/K.m^2$ to 26000 $W/K.m^2$ [22, 26]. Hence, microchannel heat-exchangers which is approximately 80 % smaller than a shell-and-tube heat-exchanger in terms of size and weight, provides similar heat transfer properties [22, 38]. Higher surface to volume ratios also allows proper temperature control along the channel length, which hinders possible hot spot formation [35]. Scaling up the microchannel heat-exchangers for the desirable heat transfer is one of the major advantages of the

microchannel heat-exchangers in terms of practicality and operation safety. In doing so, possible adverse effects are prevented when converting the system from the pilot-scale to commercial size.

Ceramic, stainless steel and certain polymers are preferred as wall material in the construction microchannel heat-exchanger [39]. Materials of construction also dictate fabrication techniques which are reviewed extensively in the literature [35]. It is also reported that rectangular and triangular cross sections are the most widely used microchannel geometries [35].

Despite the benefits, microchannel heat-exchangers pose certain challenges in manufacturing and modeling. Micro-scale height and the geometry of the channels have negative impacts on the pressure drop which inherently increases the need for pumping power [40]. Moreover, fabrication techniques require high purified raw material especially in molding methods, and also advanced engineering techniques which increase in manufacturing costs [35]. The flow of the fluids in the channels is performed under laminar regime due to hydraulic diameters in the order of micrometers. In this case, both convective and diffusive terms in mass and heat transport have to be taken into account. This requirement makes mathematical modeling of the microchannel units complicated [39,41]. With these characteristics, the microchannel heat-exchanger is implemented to the cascade reactor system configuration for a proper temperature regulation of the hot reactor effluent.

## 2.2. DME Synthesis

DME synthesis takes places via the reactions expressed as follows with the addition of syngas mixture consisting of CO, $CO_2$ and $H_2$ homogeneously [20]:

Methanol synthesis 1 ($MS_1$):

$$CO + 2\,H_2 \rightleftharpoons CH_3OH \qquad \Delta H^0 = -90.4 \text{ kJ mol}^{-1} \qquad (2.1)$$

Methanol synthesis 2 ($MS_2$):

$$CO_2 + 3\,H_2 \rightleftharpoons CH_3OH + H_2O \qquad \Delta H^0 = -49.4 \text{ kJ mol}^{-1} \tag{2.2}$$

Methanol dehydration 3 (MD):

$$2\,CH_3OH \rightleftharpoons CH_3OCH_3 + H_2O \qquad \Delta H^0 = -23.0 \text{ kJ mol}^{-1} \tag{2.3}$$

The combination of $MS_1$ and $MS_2$ reactions results in the implicit reverse water gas shift reaction, which reaches equilibrium simultaneously [19]. The amount of water produced from RWGS is highly correlated with respect to $CO_2$ composition in the feed.

Reverse water-gas shift (RWGS):

$$CO_2 + H_2 \rightleftharpoons CO + H_2O \qquad \Delta H^0 = 41.0 \text{ kJ mol}^{-1} \tag{2.4}$$

Due to the high exothermicity of the Reactions 2.1- 2.3, methane formation is inevitable in case of temperature rise above 573 K.

Methane Formation (MD):

$$CO + 3\,H_2 \rightleftharpoons CH_4 + H_2O \qquad \Delta H^0 = -206.0 \text{ kJ mol}^{-1} \tag{2.5}$$

Dimethyl ether synthesis can be carried out by the so-called indirect (two-step) and direct (single step) routes [12]. In the indirect route, syngas - mixture of carbon oxides and hydrogen - conversion is firstly converted to methanol typically on a Cu-$ZnO/Al_2O_3$ catalyst. The methanol dehydration, on the other hand, is carried out in a separate, consecutive reactor via the use of $\gamma$–$Al_2O_3$ or HZSM-5 catalyst, , both of

which are relatively acidic compared to Cu-$ZnO/Al_2O_3$ [19]. The single-step process combines methanol synthesis and dehydration reactions in a single reactor loaded with either the physical mixture of the methanol synthesis and dehydration catalysts or a bifunctional catalyst involving the co-existence of the synthesis and dehydration functions on the same support [10, 18]. Overall, the single-step route is more advantageous in terms of methanol and DME formation since the combination of both formation and deactivation of methanol enables more syngas conversion which is restricted by the thermodynamic constraints in the indirect route [19].

### 2.2.1. Indirect DME Synthesis

The indirect route forms the basis of the current technology of making DME at an industrial scale. Indirect synthesis consists of two consecutive steps [20]. In the first step, methanol production is carried out in the first reactor, followed by a separator to purify methanol for step two. Secondly, purified methanol is used in order to produce DME in the following reactor [12, 42]. Operating temperature is set below 573 K in order to increase DME yield and selectivity and prevent $CH_4$, and coke formation [12]. However, due to thermodynamic constraints, indirect route results in lower single-pass conversion [12]. Another drawback of the indirect method is the capital and operating cost of the two reactors and separators [34]. Overall, indirect synthesis provides practical separation and hence higher DME selectivity [12]. TOYO company, which embarked on the indirect DME production from coal-based syngas in 2003, possess four plants having capacity within the range of 110,000 t/y to 210,000 t/y in China [43].

In order to produce DME commercially with the production rate of 3000 t/d, Lurgi developed a new process called Lurgi MegaDME® process, which enables a significant reduction in both investment cost and energy consumption [44]. The main advantage of this process is that methanol distillation in the Lurgi route is not required as opposed to the conventional DME processes [44]. The schematic route of called Lurgi MegaDME® process is shown in Figure 2.4:

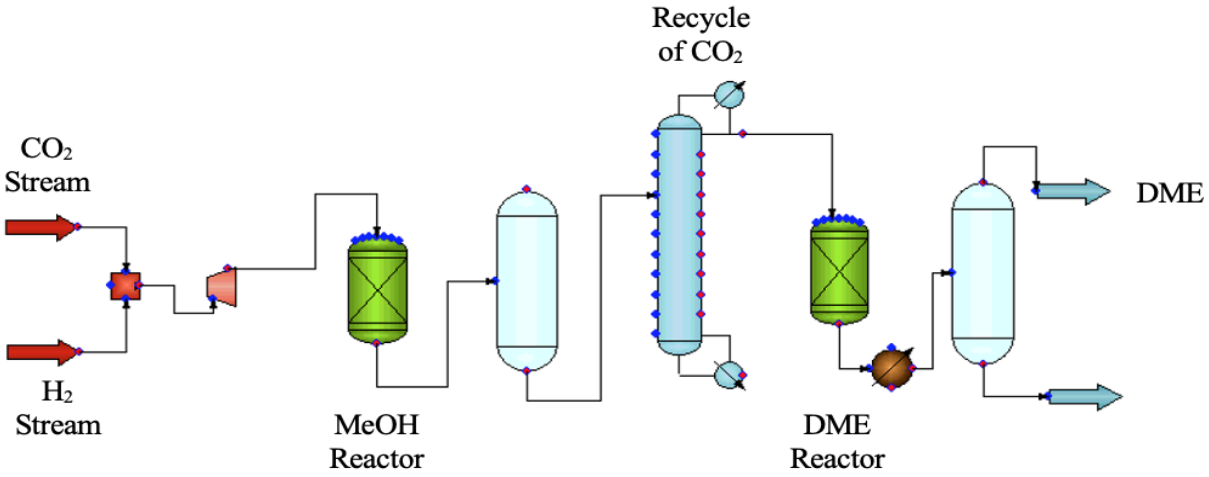


Figure 2.3. The indirect synthesis scheme [44]

Previous studies on DME synthesis have provided the effect of different parameters such as pressure (1-100 bar) $H_2/CO$ (0.5-2.5) ratio, and temperature (473-593 K) onto the syngas conversion and DME yield [17]. The $CO_2$ conversion and DME yield are expressed within the range of 10-100 and 20-97% respectively [17, 20].

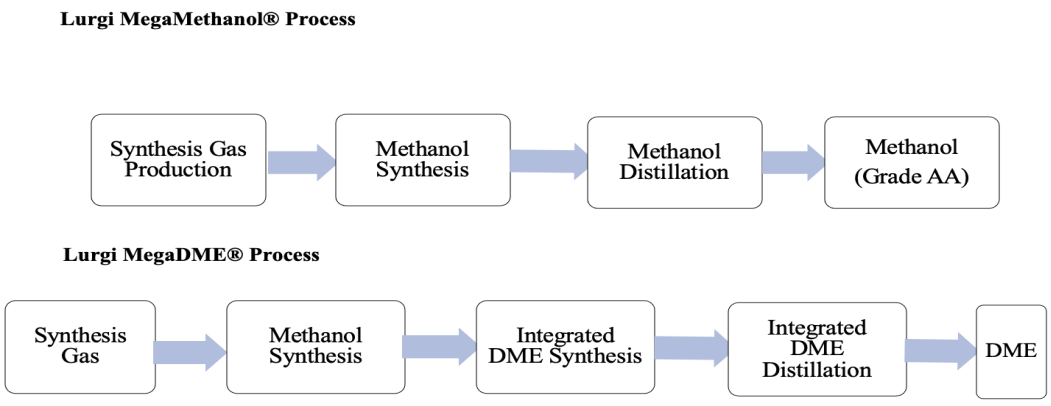


Figure 2.4. The Lurgi synthesis scheme (adapted from [44]).

Zhu *et al.* [45] conducted an experimental study on indirect DME synthesis with two-consecutive packed-beds loaded with CZA and HZSM-5 catalysts for methanol

synthesis and DME synthesis respectively. The reactor temperature varies between 543–553 in the first step and 488–498 K in the second step [45]. $H_2$/CO is kept at 2, and pressure is set to 80 bar in order to obtain higher CO conversion and DME yield up to 78 and 63% respectively [45]. As opposed to methanol synthesis reactions, DME synthesis via Reaction 2.3 is pressure independent. Under thermodynamic limitations, 70–85 % conversion of methanol per pass can be achieved at 523-633 K depending on the water content of the reactor feed [44].

### 2.2.2. Direct DME Synthesis

One step DME production process has been an innovative approach for researchers [20,46]. In this method, both syngas conversion and DME formation reactions are carried out in a single reactor. A sudden consumption of methanol, which, firstly results in thermodynamically favoured syngas conversion, in turn, leads to the evolution of more exothermic heat necessitating precise temperature control [19]. Moreover, physical contact of the catalysts induces the risk of deactivation through the exchange of the metallic functions [19]. However, single step DME synthesis offers process intensification with significant reductions in the capital and operating expenditures since in-situ methanol conversion to DME stimulates the thermodynamically limited methanol synthesis reactions [20]. Several studies on direct DME synthesis are reported with different reactor configurations in the literature.

Copper-zinc based catalysts feature stimulating attributes in the methanol formation reactions [47]. The ratio of $Cu^+$ to $Cu^\circ$, which affect the active sites and, in turn, syngas conversion, can be adjusted via ZnO amount added into the catalyst [19]. On the other hand, the copper-zinc catalyst has an inhibiting effect on the reverse water gas shift reaction (RWGS) which occurs implicitly with the combination of CO and $CO_2$ based methanol synthesis. It should be noted that a serious catalyst deactivation can be observed in excess of ZnO catalyst [34, 48]. The performance and stability of the Cu-ZnO catalyst can be improved with the addition of metallic supports such as Al and Pd [2,34]. With this bimetallic catalyst combination, possible catalyst sintering can also be mitigated. In terms of cost and performance, CZA is more prevalent among

the industry [49]. The optimum operating condition for CZA is suggested between 50 to 100 bar and 513-523 K isothermally [46, 50, 51]. The biggest threatening problem on CZA stems from the water generation in the $CO_2$ based methanol formation due to the hydrophilic composition of $Al_2O_3$ [2]. To combat this issue, CZA can be enhanced with the addition of $ZrO_2$ which reduces the hydrophilicity of the catalyst [2, 46].

The literature reviews illustrate that $\gamma$-$Al_2O_3$ and HZSM-5 catalysts perform relatively higher in terms of stability, activity and the selectivity of the DME in a methanol dehydration reaction [2, 46]. $\gamma$-$Al_2O_3$ stands for its lower cost compared to other commercial catalysts, weak to moderate acid sites and hydrophobic surface required for the DME synthesis [2,46,52]. $\gamma$-$Al_2O_3$ shows an impressive performance in mechanical and thermal stability [2,52]. The major drawback of this catalyst is that it requires a higher operating temperature than 523 K in order to maintain the system in favour of methanol dehydration [2,12,32]. In that way, owing to weak Lewis acid sites, DME selectivity percentage can be enhanced even around 673 K [2,52]. Also, the fact that water formation in the methanol dehydration and methanol formation reactions adversely affect $\gamma$-$Al_2O_3$ stability due to strong tendency of water adsorption [2,53–57].

HZSM-5 is another methanol dehydration catalyst which delivers outstanding resistance to water adsorption owing to its medium to strong Lewis and/or Brønsted type acid sites. As opposed to $\gamma$-$Al_2O_3$, HZSM-5 catalyst favours lower temperature operating range around 503 K [2]. Vishwanathan *et al.* [58] investigated the effect of temperature on the methanol conversion and indicated that the methanol conversion is estimated approximately 80 % at 503 K with the use of HZSM-5 catalyst whereas the same conversion is obtained for $\gamma$-$Al_2O_3$ at 503 K [2,58]. Hence, this indicates HZSM-5 is more favourable in terms of economic and thermodynamic concerns. On the other hand, the major issue of HZSM-5 is the coke formation and a significant drop in DME selectivity due to strong acid sites [2]. To tackle this problem, the impregnation of certain metals such as Na, Zn, Zr onto HZSM-5 is applied to reduce the strength of the acidity of sites [2].

Naik *et al.* [2,52] conducted comparative studies on the catalytic activity CZA+$\gamma$-$Al_2O_3$ and CZA+HZSM-5 in a fixed-bed reactor operated isothermally at 533 K and 50 bar. As a result of the direct synthesis of $CO_2$ to DME, the conversion and DME selectivity for both catalysts are reported as 20 and 30 %, 5 and 75 % respectively [52]. This study illustrates that the stability of CZA+$\gamma$-$Al_2O_3$ is adversely affected in the presence of $CO_2$ forming a dramatic amount of water in methanol formation [52].

Moradi *et al.* [59] simulated a 3D fixed-bed reactor model on direct DME synthesis via the most widely used CFD software ANSYS. The studies comprise both isothermal and adiabatic simulations for 523 to 553 K and 40 to 60 bar with the CZA+$\gamma$-$Al_2O_3$-$ZrO_2$ catalyst to explore the temperature change effect onto the conversion and operating conditions [59]. The optimum conditions for CO and $H_2$ are 543 K and 50 bar and 533 K , 50 bar under adiabatic and isothermal conditions. DME selectivity reaches above 80 % in both cases with $CO/H_2$ ratio 1, and maximum conversion acquires 86.2 for the isothermal case [59].

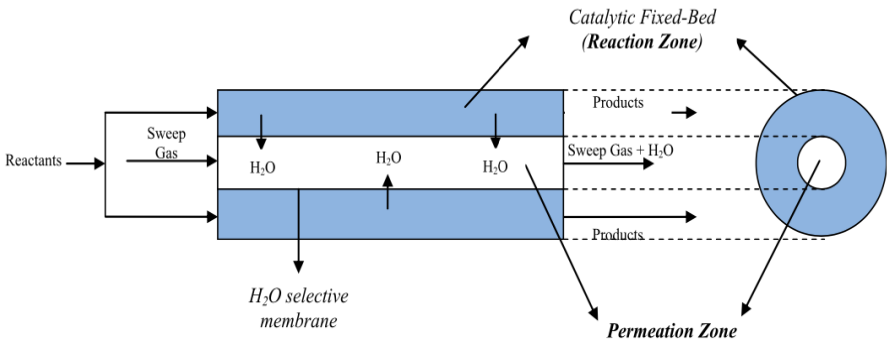


Figure 2.5. Membrane fixed-bed reactor configuration scheme [60].

As mentioned earlier, water formation has an inhibitive impact on the DME synthesis process. De Falco *et al.* [60] investigated the effect of the water removal on the direct DME synthesis from syngas under the operating conditions of 473-548 K and 20-70 bar for CZA+HZSM-5 catalyst in the 1D non-isothermal microporous zeolite membrane reactor . The CO, $CO_2$ conversion and DME yield is reported as 75, 69 and 75 % with membrane configuration under 70 bar, 500 K with the syngas ($CO_2$/CO)

ratio of 3 and GHSV of 7000 $h^{-1}$ [60]. The enhancement of the syngas conversion and DME yield with membrane configuration compared to the conventional bed reactor is indicated as 30 % on average [60, 61].

Due to the high exothermicity of the methanol formation and dehydration reactions, proper temperature control paves the way for the novel designs for this challenge. Vakili *et al.* [15] comes up with a numerical thermally coupled reactor model. Syngas stream is fed to the tubes cocurrent with water fed in the shell side. The reactions are carried out at 493 K and 50 bar with a composition of the effluent of the natural gas facility with CZA+$\gamma$-$Al_2O_3$ (1:1 mass ratio) [15]. The annual capacity of this design it is reported as 600 ton which is promising for the future mass-scale production [15]. The configuration of the catalytic heat-exchanger reactor is illustrated below. Hu *et al.* [62] has also studied the syngas conversion and DME selectivity percentage in the shell and tube heat-exchanger reactor loaded with CZA+$\gamma$-$Al_2O_3$. Similar to Vakili *et al.*, Hu *et al.* [62] also provides the required cooling with water [62–64]. According to this study, the CO conversion and DME selectivity are obtained as 57.5 and 83 % respectively and an annual production of 102,800 and 14,800 tons DME and methanol [10, 62].

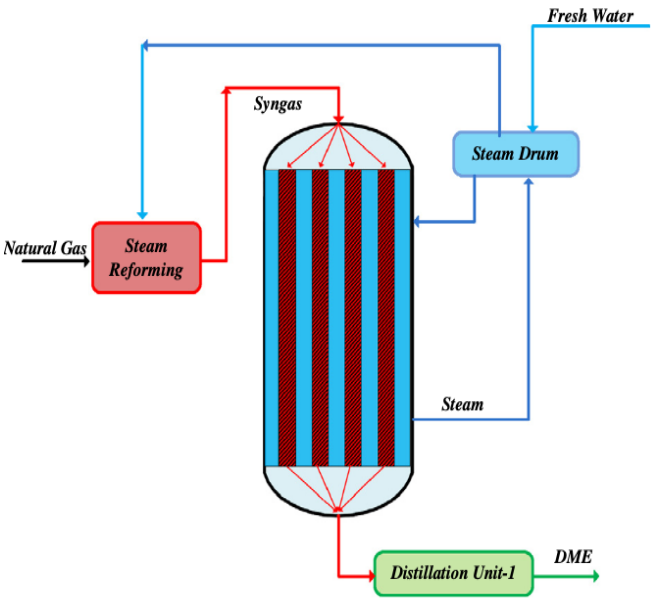


Figure 2.6. Thermally coupled reactor configuration scheme [15].

Bai *et al.* [65] investigated 1D pseudo-homogeneous adiabatic packed-bed reactors with interstage quenching for direct DME synthesis at the temperature and pressure range of 513–553 K and 6-18 bar with the annual production capacity of 210,000 tons. From the paper, the methanol conversion and DME yield are obtained as 84 and 42 % respectively at 533 K and 12 bar [34, 65].

Slurry reactors are an alternative configuration which is commercially operated in the DME synthesis. Papari *et al.* [66] simulated a 3 phase homogeneous and heterogeneous models for mass-scale at the range of 513-553 K and 40-60 bar. Based on the presented results, the production capacity is stated as 3800 tons/day under 533 K and 60 bar with the reactor height and weight of 7 and 50 m respectively [66].

Microchannel reactors have become dominant in the process intensification of the DME synthesis. Hayer *et al.* [37] have conducted both experimental and 2D pseudo-homogeneous model studies with the catalyst of CZA+$\gamma$-$Al_2O_3$. The operating conditions vary within the range of 483 to 573 K, 10 to 50 bar, 4500-60000 ml/gcat/h and 1 to 4 in terms of $H_2$/CO ratio [12, 37]. The experimental results illustrate that the highest conversion is obtained at 523 K and 50 bar with the $H_2$/CO ratio of 2 [37]. Furthermore, Hu *et al.* [67] performed experimental research on DME synthesis with respect to different methanol dehydration catalyses such as HZSM-5, acidic $Al_2O_3$ and F-$Al_2O_3$ with the combination of methanol synthesis catalyst, F51-8PPT (Kataco Corp.). During the experiments, a biomass-based composition is fed to the microchannel reactor under the operating conditions of 38 bar and 553 K [67]. The DME selectivity and syngas conversion are reported for each catalyst within the range of 60.2 to 63 % and around 80 % respectively [67].

In the context of the this research, direct (one–step) DME production from syngas containing $CO_2$ will be modelled and simulated in the cascade reactor configuration.The overall reactions are highly exothermic which takes places in adiabatic packed-bed reactors, hence the balance between thermodynamics and kinetics should be optimized via maintaining temperature control with the microchannel heat-exchangers. By optimizing the size and number of catalytic beds and heat-exchangers, temperature evolution

of the entire process can be regulated efficiently. The lack of such an approach in direct DME synthesis sets the motivation for the proposal of this study.

# 3. MATHEMATICAL MODELING AND SIMULATION

## 3.1. Cascade reactor system

The cascade reactor system consists of serial adiabatic packed-bed reactors loaded with the physical mixture of the catalysts for methanol synthesis (Cu-ZnO/$Al_2O_3$ (CZA)) and methanol dehydration ($\gamma$-$Al_2O_3$ or HZSM-5). Between each packed-bed reactor, microchannel heat- exchangers composed of rectangular shaped-channels are placed to regulate the reaction temperature (i.e. to reduce the temperature elevated by the exothermic heat released in the preceding adiabatic reactor).

In this chapter, the mathematical modelling and simulation of cascade reactor system for the direct (one–step) synthesis of DME from syngas containing $CO_2$ is explained. In Section 3.1.1, the information on the reactor configuration, working equations (material, energy and momentum balances), initial conditions as well as the assumptions are provided. Working equations (Navier-Stokes equations), boundary conditions and the assumptions on microchannel heat-exchangers are presented in Section 3.1.2. Information regarding the reaction and kinetic modelling of direct synthesis of DME is stated in Section 3.2.

### 3.1.1. Adiabatic Packed-Bed Reactor Design

In the design of cascade reactor configuration, 1D-pseudo homogeneous model of the packed-bed Reactor (PBR) is constructed meaning that reaction in the system takes place at only gaseous phase [29]. However, in reality, all the reactions occur on the catalyst surface, which is proportional to the amount of catalyst packed into the bed. Based on the 1D-pseudo homogeneous assumption, the material, energy and momentum balances for packed-bed reactors are expressed in the following subsections. The axial flow assumption is also made during the PBR modeling meaning that both the reaction and the flow of the species vary with respect to axial direction only.

Before determining the dimensions of the PBR, first of all, the molar flow-rate fed to the $1^{st}$ packed-bed reactor is calculated based on the literature [68]. According to Wan *et al.* [68], the wood chip consumption rate and syngas yield are reported as 26.5 kg-wood/h and 2.5 $Nm^3$gas/kg-wood. From the wood chip consumption rate and syngas yield, effluent syngas's normal volumetric flow-rate is calculated from Equation 3.1 [69].

$$Q_{vol,syn} = yield_{syn} \times m_{w.chip} \tag{3.1}$$

From the volumetric flow-rate, molar flow-rate of the first bed in the cascade reactor system is calculated by using ideal gas law in Equation 3.2.

$$F_0 = \frac{P_N \times Q_{vol,syn}}{R \times T_N} \tag{3.2}$$

Based on the calculations stated above, the inlet molar flow rate of Bed-1 is determined as 0.82 mol/s.

During the design of the cascade reactor system, the determination of the weight of catalyst loaded in the packed-bed is done via trial and error in a way that the outlet temperature of the reactor should not exceed 543 K [15, 20, 24]. The maximum temperature is chosen based on the prevention of catalyst deactivation of CZA catalyst as well as undesired methane formation (Reaction 2.5). For a given mass of catalyst, the optimization of L and D are done by using Equations 3.3−3.5 with the consideration of pressure drop [29, 61].

$$V_{cat} = \frac{w_{cat}}{\rho_{cat}} \tag{3.3}$$

$$\rho_{cat} = \frac{\rho_{bulk}}{1 - \epsilon} \tag{3.4}$$

where $\rho_{bulk}$ refers to 1273 and 1200 kg/m$^3$ for CZA+$\gamma$-$Al_2O_3$ and CZA+HZSM-5 catalysts respectively [15, 18, 61].

$$V_{reac} = \frac{w_{cat}}{1 - \epsilon} \tag{3.5}$$

where $\epsilon$ stands for the porosity of the catalytic bed, taken as 0.39 for both catalysts [61].

As a result of the estimations, the packed-bed diameter is chosen as 0.025 m for both CZA $-$ $\gamma Al_2O_3$ and CZA+HZSM-5 catalysts. Since the catalysts possess different bulk density, the reactor length with the specified diameter is calculated as 0.275 and 0.291 m respectively from Equations 3.6$-$3.7.

$$A_c = \frac{D_{in}^2 \pi}{4} \tag{3.6}$$

$$L_{reac} = \frac{V_{reac}}{A_c} \tag{3.7}$$

3.1.1.1. Material Balance in Packed-Bed Reactors. The general material balance equation is expressed in Equation 3.8:

$$Accumulation = In - Out + Generation - Consumption \tag{3.8}$$

Since the process is carried out at steady state, accumulation is equal to 0. By dividing both sides by $\Delta w_{cat}$ to obtain Equation 3.9 :

$$r_i = \frac{F_{i,w_{cat}} - F_{i,(w_{cat}+\Delta w_{cat})}}{\Delta w_{cat}} \tag{3.9}$$

The general mole balance for PBR is stated in Equation 3.10 and illustrated in Figure 3.1.

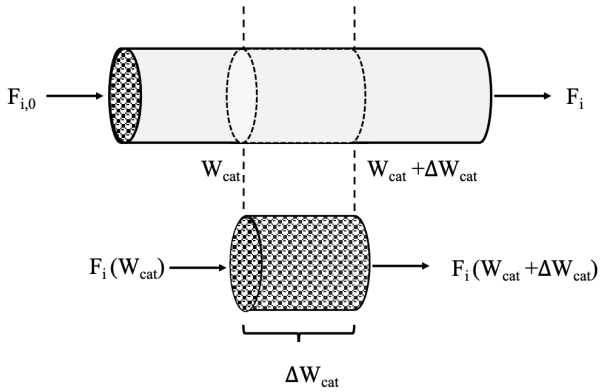


Figure 3.1. Packed-bed reactor scheme.

$$\frac{dF_i}{dt} = F_{i,W_{cat}} - F_{i,(W_{cat}+\Delta W_{cat})} + r_i \times \Delta w_{cat} \tag{3.10}$$

By using the definition of derivative in terms of limit shown in Equation 3.11, differential form of mole balance on a PBR at steady state is derived as shown in Equation 3.12:

$$\lim_{\Delta w_{cat}\to 0}\left[\frac{F_{i,w_{cat}} - F_{i,(w_{cat}+\Delta w_{cat})}}{\Delta w_{cat}}\right] = \frac{dF_i}{dw_{cat}} \tag{3.11}$$

$$\frac{dF_i}{dw_{cat}} = r_i \tag{3.12}$$

The mole balance for each species are specified between the Equations 3.13−3.18:

CO material balance:

$$\frac{d_{\mathrm{CO}}}{dw_{cat}} = R_{\mathrm{CO}} = -r_{MS_1} \tag{3.13}$$

$H_2$ material balance:

$$\frac{d_{H_2}}{dw_{cat}} = R_{H_2} = -2r_{MS_1} - 3r_{MS_2} \tag{3.14}$$

$CO_2$ material balance:

$$\frac{d_{CO_2}}{dw_{cat}} = R_{CO_2} = -r_{MS_2} \tag{3.15}$$

$H_2O$ material balance:

$$\frac{d_{H_2O}}{dw_{cat}} = R_{H_2O} = r_{MS_2} + r_{MD} \tag{3.16}$$

$CH_3OH$ material balance:

$$\frac{d_{CH_3OH}}{dw_{cat}} = R_{CH_3OH} = r_{MS_1} + r_{MS_2} - 2r_{MD} \tag{3.17}$$

$CH_3OCH_3$, DME material balance:

$$\frac{d_{CH_3OCH_3}}{dw_{cat}} = R_{CH_3OCH_3} = r_{MD} \tag{3.18}$$

CO, $CO_2$ conversion and DME yield percentages are calculated based on Equations 3.19−3.21:

$$\chi_{CO} = \frac{F_{CO,0} - F_{CO}}{F_{CO,0}} \times 100 \tag{3.19}$$

$$\chi_{\mathrm{CO_2}} = \frac{F_{\mathrm{CO_2},0} - F_{\mathrm{CO_2}}}{F_{\mathrm{CO_2},0}} \times 100 \tag{3.20}$$

$$\mathrm{DME}_{yield} = \frac{2 \times F_{\mathrm{CH_3OCH_3}}}{F_{\mathrm{CO},0} + F_{\mathrm{CO_2},0}} \times 100 \tag{3.21}$$

3.1.1.2. Energy Balance in Packed-Bed Reactors. In the simulation of the adiabatic packed-bed reactors of the cascade system, it is assumed that both the inputs and response variables are only length dependent meaning that there is no radial gradients in the context of energy balances. The general energy balance equation is expressed as follows:

$$\frac{dE_{sys}}{dt} = \dot{Q} - W + F_{in} \times E_{in} - F_{out} \times E_{out} \tag{3.22}$$

$$W = \sum_{i=species}^{n} (F_{in} \times PV_{in,i} - F_{out} PV_{out,i}) + W_s \tag{3.23}$$

where $\mathrm{E_i}$ stands for the combination of kinetic, potential and internal energy as stated in Equation 3.24. In this system, the effects of both kinetic and potential energy are negligible, hence only internal energy term is taken into consideration in the energy balance as shown in the second part of Equation 3.24 :

$$E_i = U_i + g \times z_i + \frac{u_i^2}{2} \qquad E_i = U_i \tag{3.24}$$

To calculate state properties with respect to temperature, the internal energy is expressed in terms of enthalpy change of species as follows:

$$H_i = U_i + PV_i \tag{3.25}$$

So, inlet enthalpy and outlet enthalpy of each species can be calculated in terms of internal energy by Equation 3.26.

$$F_i \times H_i = F_i \left(U_i + PV_i\right) \tag{3.26}$$

By combining Equations 3.22 and 3.26, also knowing that there is no mechanical work applied from/to the system, energy balance for a steady-state adiabatic system can be obtained in terms of enthalpy change ($\Delta$H).

$$0 = \sum_{i=species} F_{i,in} \times H_{i,in} - \sum_{i=species} F_{i,out} \times H_{i,out} \tag{3.27}$$

To calculate reaction enthalpies, Gibbs free energy and entropies, both of the formation of properties and the stoichiometric coefficients of each species are required [70].

$$\Delta H_{rxn} = \sum_{i=products} \upsilon_i H_{f,i} - \sum_{i=reactants} \upsilon_i H_{f,i} \tag{3.28}$$

$$\Delta G_{rxn} = \sum_{i=products} \upsilon_i G_{f,i} - \sum_{i=reactants} \upsilon_i G_{f,i} \tag{3.29}$$

In order to calculate enthalpies, Gibbs free energy and entropies, equations 3.30, 3.32−3.36 have to be evaluated in terms of kJ.mol$^{-1}$ and kJ.mol$^{-1}$.K$^{-1}$. The constants for the calculation of the heat capacity, enthalpy, entrophy and Gibbs free energy are tabulated in Table 3.1:

$$\frac{c_{p,i}}{R} = a_1 + a_2 T + a_3 T^2 + a_4 T^3 + a_5 T^4 \tag{3.30}$$

Table 3.1. Heat capacity constants for enthalpy (ΔH), entropy (ΔS), and Gibbs free energy (ΔG) calculations [71].

| Species ($i$) | $a_1$ | $a_2(\times 10^3)$ | $a_3(\times 10^6)$ | $a_4(\times 10^9)$ | $a_5(\times 10^{12})$ | $b_1(\times 10^{-4})$ | $b_2$ |
|---|---|---|---|---|---|---|---|
| CO | 3.58 | -0.61 | 1.02 | 0.91 | -0.90 | -1.43 | 3.51 |
| $H_2$ | 2.34 | 7.98 | -19.50 | 20.20 | -7.38 | -0.092 | 0.68 |
| $CO_2$ | 2.36 | 8.98 | -7.12 | 2.46 | -0.14 | -4.84 | 9.90 |
| $H_2O$ | 4.20 | -2.04 | 6.52 | -5.49 | 1.77 | -3.03 | -0.85 |
| $CH_3OH$ | 5.72 | -15.20 | 65.20 | -71.10 | 26.10 | -2.56 | -1.50 |
| $CH_3OCH_3$ | 5.31 | -2.14 | 53.10 | -62.30 | 23.10 | -2.40 | 7.13 |
| $CH_4$ | 5.15 | -13.70 | 49.20 | -48.50 | 16.70 | -1.02 | -4.64 |
| $N_2$ | 0.35 | 0.00 | 0.00 | 2.44 | -1.41 | -0.10 | 2.97 |

$$\frac{H_{f,i}}{RT} = a_1 + a_2\frac{T}{2} + a_3\frac{T^2}{3} + a_4\frac{T^3}{4} + a_5\frac{T^4}{5} + \frac{b_1}{T} \tag{3.31}$$

$$H_{f,i} = \{a_1 + a_2\frac{T}{2} + a_3\frac{T^2}{3} + a_4\frac{T^3}{4} + a_5\frac{T^4}{5} + \frac{b_1}{T}\} \times (RT) \tag{3.32}$$

$$\frac{S_{f,i}}{R} = a_1 InT + a_2 T + a_3\frac{T^2}{2} + a_4\frac{T^3}{3} + a_5\frac{T^4}{4} + \frac{b_1}{T} \tag{3.33}$$

$$S_{f,i} = R \times \left(a_1 InT + a_2 T + a_3\frac{T^2}{2} + a_4\frac{T^3}{3} + a_5\frac{T^4}{4} + \frac{b_1}{T}\right) \tag{3.34}$$

$$\frac{G_{f,i}}{RT} = \frac{H_{f,i}}{RT} - \frac{S_{f,i}}{R} \tag{3.35}$$

$$G_{f,i} = (RT) \times \left( \frac{H_{f,i}}{RT} - \frac{S_{f,i}}{R} \right) \tag{3.36}$$

By combining Equations 3.27, 3.28 ,3.32, energy balance can be written in terms of conversion and rate of reactions [29].

$$\sum_{i=species} (F_{i,in}H_{i,in} - F_{i,out}H_{i,out}) = F_{\mathrm{CO},0} \sum_{i=species} \upsilon_i H_{in,i} - \upsilon_i H_{out,i} - \Delta H_{rxn}\chi_{CO} \tag{3.37}$$

By combining Equations 3.12, 3.32 and 3.37, the following equation (i.e. the differential energy balance for adiabatic packed-bed reactors) is obtained and used for computing temperature of the packed-bed reactor with respect to the weight of catalyst [29]:

$$\frac{dT}{dw_{cat}} = \frac{\sum_{j=rxn} (\Delta H_{rxn} \times -r_{rxn,j})}{\sum_{i=species} (F_i \times c_{p,i})} \tag{3.38}$$

3.1.1.3. Momentum Balance in Packed-Bed Reactors. The pressure drop of the gas flowing within a packed-bed can be calculated via Ergun's Equation [29]:

$$\frac{dP}{dL} = -\frac{G}{\rho_m D_p} \left( \frac{1-\epsilon}{\epsilon^3} \right) \left[ \frac{150(1-\epsilon)\mu_m}{D_p} + 1.75G \right] \tag{3.39}$$

In Equation 3.39, G stands for the superficial mass velocity, which is defined below:.

$$G = \rho_m . u \tag{3.40}$$

Ergun's equation can be expressed in terms of catalyst weight as follows [29]:

$$\frac{dP}{dw_{cat}} = -\frac{\beta_0}{\rho_{cat} A_c (1-\epsilon)} \tag{3.41}$$

$$\beta_0 = \frac{G}{\rho_m D_p}\left(\frac{1-\epsilon}{\epsilon^3}\right)\left[\frac{150(1-\epsilon)\mu_m}{D_p} + 1.75G\right] \tag{3.42}$$

In order to calculate the pressure drop using Equation 3.41, viscosity of the mixture should be computed. Due to the high pressures involved in DME synthesis, the effect of pressure should be taken into account. The following set of correlations are used to evaluate gas phase viscosity at high pressures:

$$\mu_r = 131.3\frac{\delta}{(V_c T_c)^{1/2}} \tag{3.43}$$

$$\Omega_v = \left[A\left(T^*\right)^{-B}\right] + C\left[exp\left(-DT^*\right)\right] + F\left[exp\left(-FT^*\right)\right] \tag{3.44}$$

$$T_r = \frac{T}{T_c} \tag{3.45}$$

$$T^* = 1.2593 \times T_r \tag{3.46}$$

$$F_c = 1 - 0.2756\omega + 0.059035\mu_r^4 + \kappa \tag{3.47}$$

Constants needed to evaluate Equations 3.43-3.47 are provided in Tables 3.2, 3.3 and 3.4.

Table 3.2. Physical properties of species [72].

| Species ($i$) | MW (g/mol) | Dipole (debye) | $T_c$(K) | $V_c$($cm^3$/mol) | w | $\kappa$ |
|---|---|---|---|---|---|---|
| CO | 28.01 | 0.1 | 132.85 | 93.1 | 0.045 | 0.068 |
| $H_2$ | 2.0155 | 0 | 32.98 | 64.2 | -0.217 | 0.068 |
| $CO_2$ | 44.01 | 0 | 304.12 | 94.07 | 0.225 | 0.068 |
| $H_2O$ | 18.015 | 1.8 | 647.14 | 55.95 | 0.344 | 0.076 |
| $CH_3OH$ | 32.04 | 1.7 | 512.64 | 118 | 0.565 | 0.215 |
| $CH_3OCH_3$ | 46.07 | 1.3 | 400.1 | 170 | 0.281 | 0.068 |
| $CH_4$ | 16.04 | 0 | 190.56 | 98.6 | 0.011 | 0.068 |
| $N_2$ | 14.0067 | 0 | 126.2 | 90.1 | 0.037 | 0.068 |

Table 3.3. Viscosity collision integral constants [72].

| | |
|---|---|
| A | 1.16145 |
| B | 0.14874 |
| C | 0.52487 |
| D | 0.7732 |
| E | 2.161178 |
| F | 2.43787 |

The high pressure viscosity value is calculated in Equation 3.54. The computation of the required parameters are shown as follows:

$$E_i = a_i + b_i\omega + c_i\mu_r^4 + d_i\kappa \tag{3.48}$$

$$y = \frac{\rho V_c}{6} \tag{3.49}$$

$$G_1 = \frac{1 - 0.5y}{(1-y)^3} \tag{3.50}$$

Table 3.4. High pressure viscosity coefficients [72].

| j | $a_j$ | $b_j$ | $c_j$ | $d_j$ |
|---|---|---|---|---|
| 1 | 6.324 | 50.412 | -51.68 | 1189 |
| 2 | 0.00121 | -0.001154 | -0.006257 | 0.03728 |
| 3 | 5.283 | 254.209 | -168.48 | 3898 |
| 4 | 6.623 | 38.096 | -8.464 | 31.42 |
| 5 | 19.745 | 7.63 | -14.354 | 31.53 |
| 6 | -1.9 | -12.537 | 4.985 | -18.15 |
| 7 | 24.275 | 3.45 | -11.291 | 69.35 |
| 8 | 0.7972 | 1.117 | 0.01235 | -4.117 |
| 9 | -0.2382 | 0.0677 | -0.8163 | 4.025 |
| 10 | 0.06863 | 0.3479 | 0.5926 | -0.727 |

$$G_2 = \frac{\left(E_1\left[1 - exp(-E_4 y)\right]/y\right) + E_2 G_1 exp(E_5 y) + E_3 G_1}{E_1 E_4 + E_2 + E_3} \tag{3.51}$$

$$\mu^{**} = E_7 y^2 G_2 \;\; exp[E_8 + E_9 (T^*)^{-1} E_{10} (T^*)^{-2}] \tag{3.52}$$

$$\mu^* = \frac{(T^*)^{1/2}}{\Omega_v}\{F_c[(G_2)^{-1} + E_6 y]\} + \mu^{**} \tag{3.53}$$

$$\mu_i = \mu^* \frac{36.344(MT_c)^{1/2}}{V_c^{2/3}} \tag{3.54}$$

Finally, mixture viscosity is obtained from Wilkes equations in Equations 3.55 and 3.56:

$$\phi_{ij} = \frac{\left[1 + \left(\frac{\mu_i}{\mu_j}\right)^{1/2} + \left(\frac{M_{A_i}}{M_{A_j}}\right)^{1/4}\right]^2}{\left[8\left(1 + \frac{M_{A_i}}{M_{A_j}}\right)\right]^{1/2}} \tag{3.55}$$

$$\mu_m = \sum_{i=1}^{n} \frac{y_i \mu_i}{\sum_{j=1}^{n} y_j \phi_{ij}} \tag{3.56}$$

3.1.1.4. Overview of Packed-bed Reactor Design and Numerical Solution Technique.

In the configuration of the cascade bed reactor, packed-bed reactors are responsible for carrying out DME synthesis adiabatically, and the microchannel heat-exchangers provide temperature due to to the heat release from the exothermic reactions. In the present study, the effects of inlet temperature (473-513 K), inlet pressure (20-60 bar), molar feed composition (syngas or biomass-based) composition of the physical catalyst mixture (CZA+$\gamma$-$Al_2O_3$, CZA+HZSM-5), extent of steam removal and amount of catalyst loaded in the bed on the CO and $CO_2$ conversion and DME yield will be investigated. While studying the effect of one parameter, all the remaining parameters are kept under their default values.

The 1D pseudo-homogeneous packed-bed reactor configuration is constructed based on the assumptions and conditions stated as follows:

- The construction material of the packed-beds simulated in the DME synthesis process is chosen as stainless steel 13 Cr due to its compactness and durability [31].
- All simulations are carried out at steady state and under adiabatic conditions..
- Both internal and external transport limitations are neglected.
- The flow in the packed-bed is assumed to be of plug flow type since the L/D ratio is above 10 [31].
- Physical mixtures of CZA+$\gamma$-$Al_2O_3$ and CZA+HZSM-5 (1:1 by weight in both cases) are assumed to be homogeneous.

- The length of the packed-bed reactors is determined in a way that the outlet temperature should not exceed 543 K, above which the Cu-based catalyst has the risk of thermal sintering, and the pressure drop should remain below 2.5 % per bed [15, 16, 31].
- In the first part of the packed-bed model (Section 4.1 and 4.2), the desired results (maximum attainable packed-bed number, syngas conversions, DME yield, and other properties) are calculated by neglecting the pressure drop along the packed-bed.
- The enthalpy change of the fluid is equal to the heat duty of the packed-bed reactor since there is no heat or work done to/by the system [31].
- The species in the feed are given to the packed-beds in perfectly mixed condition [29].
- Coking, catalyst deactivation as well as methanol formation are neglected as the maximum reaction temperature is set below 543 K.
- The methanol formation and dehydration reactions are all reversible and occur simultaneously [20].
- The default inlet conditions for the packed-bed reactors are 493 K, 50 bar.
- The heat capacity, viscosity, reaction kinetics and expressions, Antoine constants, fugacity, catalyst properties and porosity the molar compositions data are all taken from the literature [15, 16, 61, 71–73].

During the computation of the packed-bed reactor system, which consists mainly of 3 ODEs (species material balances, energy balance and Ergun's equations), "ode15s" solver is used from "MATLAB-R2019b" software. In the packed-bed reactor model, the ordinary differential equations comprise initial-value problem, meaning that to calculate the required outputs, only initial conditions and final length or weight of catalyst should be inserted to the compiler "ode15s". Both the general and numerical expressions for the initial conditions are tabulated for both CZA+$\gamma$-$Al_2O_3$ and CZA+HZSM-5 catalyst cases.

at z=0 ;

$$T = T_{in} \qquad P = P_{in} \qquad F_i = F_{i,in}; \tag{3.57}$$

at z=L ;

$$T = T_{out} \qquad P = P_{out} \qquad F_i = F_{i,out}; \tag{3.58}$$

### 3.1.2. Microchannel Heat-Exchanger Design

During this study, microchannel heat-exchangers are especially preferred due to their compactness and effective temperature control. Also, as mentioned earlier, the adiabatic packed-bed reactor has an undesirable drawback on pressure drop; the main aim of using the microchannel heat exchangers is to minimize the cascade system's pressure drop. Since the flow in microchannel heat-exchangers is laminar, the pressure drop along the channel is negligible. In this respect, microchannel heat-exchangers play a significant role in the optimum heat transfer and compactness of the cascade reactor system. As can be seen from the representative two-dimensional illustration 3.2, the microchannel heat-exchangers includes two types of channels, namely sweep and fluid channels separated by a solid wall. In Figure 3.2, the unit cells are grouped periodically in which the net heat flux along the y-direction onto symmetry lines is zero [20, 26, 74].

In the microchannel heat exchangers, the width, height and length of each channel are 6x$10^{-4}$, 3x$10^{-4}$ and 1.5x$10^{-2}$ m, respectively. The wall thickness within the hot and cold fluid channels is chosen as 2x$10^{-3}$ m [20, 23, 74].

During the determination of the microchannel heat-exchanger length, the temperature profile of the fluid channel concerning channel length is checked. If the fluid temperature converges at around 493.15 K with given sweep type and reactor outlet

conditions in a specific length, the channel dimension is chosen accordingly. The cross-sectional dimensions of microchannels are selected according to the transport rate considerations, which is inversely proportional to the hydraulic diameters [20, 74]. As the cross-section geometry affects Nu and Sh numbers asymptotically, the smaller the microchannel size, the higher pressure drop along the microchannel length [20, 25, 74–76].

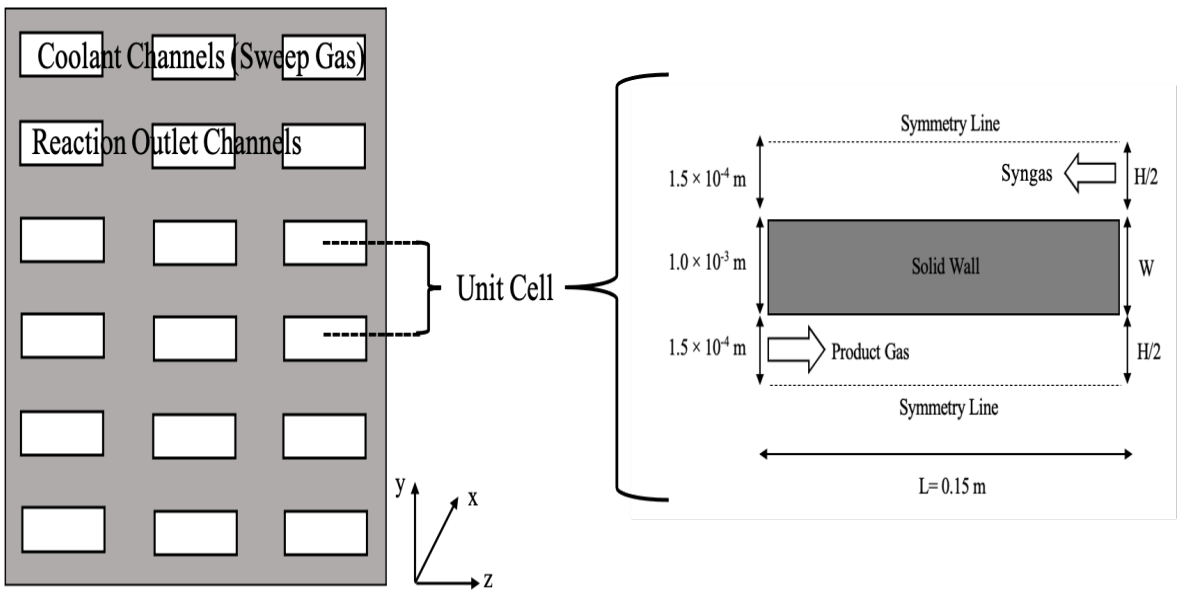


Figure 3.2. The microchannel heat-exchanger scheme [20] (drawing is not to scale).

The microchannel number depends on both the outlet flow-rate of the packed-bed reactor and the cross-sectional area of the microchannels. The inlet superficial velocity of the reaction outlet channel is chosen as 0.2 m/s by trial and error.

$$A_c = Width \times Height \tag{3.59}$$

$$Q_{vol,rxn} = u_s \times A_c \tag{3.60}$$

By using Equations 3.2 and 3.60, the molar flow-rate of a reaction outlet channel is calculated under reactor exit conditions. Finally, the number of the microchannel

is calculated by dividing the outlet flow-rate of the packed-bed by microchannel inlet molar flow-rate. In doing so, 20609 reaction outlet channel is found to provide the desired cooling.

3.1.2.1. Working Equations in Microchannel Heat-Exchanger. Modeling and simulation of the microchannel heat-exchangers are carried out by taking the following assumptions and considerations into account:

- Microchannel heat-exchangers are operated countercurrently.
- Both the fluid and sweep gas passing through each channel are defined as incompressible and Newtonian.
- The external and gravitational forces are not taken into consideration.
- The species composition and superficial velocity are homogeneously distributed at the entrance of the channel. Along the length, on the other hand, fluid properties vary due to temperature rise or drop [23].
- The laminar flow regime is valid along the length of the microchannel. Also, fully developed assumption is invalid since $1/\mathrm{Re}^2$ value is relatively higher [23, 24].
- According to the previous studies on catalytic microchannel reactors [20, 24], pressure along the microchannels remains below % 1, and therefore neglected in the present study.
- In the light of the previous studies carried out under similar conditions and channel geometries, the model equations are solved in two dimensions (2D) [23, 74].

With regard to the considerations and assumptions stated above, the model equations for quantifying the unit cell of the microchannel heat-exchanger can be given as follows:

Continuity equation:

$$\nabla.\left(\rho_m \vec{v}\right) = 0 \tag{3.61}$$

Momentum balance:

$$\nabla.\left(\rho_m \vec{v}^2\right) = -\nabla P + \nabla \cdot \left[\mu_m \left(\nabla \vec{v} + (\nabla \vec{v})^\gamma - \frac{2}{3}(\nabla \cdot \vec{v})\vec{I}\right)\right] \tag{3.62}$$

Species mass transport equations:

$$\nabla \cdot (\rho_m \vec{v} Y_i) = -\nabla \cdot \vec{J}_i \tag{3.63}$$

$$\vec{J}_i = -\rho_m D_{i,m} \nabla Y_i \tag{3.64}$$

Energy equations for gas mixture:

$$\nabla \cdot (c_{p,m} \vec{v} T_m) = \nabla \cdot (k_m \nabla T_m) \tag{3.65}$$

Energy equations for wall:

$$\nabla \cdot (k_w \nabla T) = 0 \tag{3.66}$$

Boundary conditions needed to complete the definition of the model are given as follows:

at channel entrance, z=0, $\forall$ x and $\forall$ y:

$$u = u_{in} \qquad y_i = y_{i,in} \qquad T = T_{in}; \tag{3.67}$$

at channel exit, z=L, ∀ x and ∀ y:

$$P = P_{out} \qquad \vec{n} \cdot \vec{J}_i = 0 \qquad \vec{n} \cdot (-k_m \nabla T) = 0 \tag{3.68}$$

at symmetry line, ∀ x;

$$(\vec{n} \cdot \vec{v}) = 0 \tag{3.69}$$

$$\vec{n} \cdot \left( \vec{J}_i + \rho_m \vec{v} y_m \right) = 0 \tag{3.70}$$

$$\vec{n} \cdot (-k_m \nabla T + \rho_m c_{p,m} \vec{v} y_i T_m) = 0 \tag{3.71}$$

at channel-wall interface, ∀ x;

$$(\vec{n} \cdot \vec{v}) = 0 \tag{3.72}$$

$$\left( \vec{n} \cdot \vec{J}_i + \rho_m \vec{v} y_i \right) = 0 \tag{3.73}$$

$$\vec{n} \cdot (-k_w \nabla T_w) = \vec{n} \cdot (-k_m \nabla T + \rho_m c_{p,m} \vec{v} y_i T_i) \tag{3.74}$$

The wall properties of microchannel heat-exchangers are provided in Table 3.5.

Table 3.5. Physical properties of microchannel heat-exchanger wall [77–79].

| Wall material | $\rho_w$(kg/m$^3$) | c$_p$ (J/kg.K) | ($k_w$) (W/m.K) |
|---|---|---|---|
| Cordierite | 2300 | 850 | 1.7 |
| Iron chromium alloy | 7220 | 460.55 | 58.72 |
| Stainless steel | 8030 | 502.48 | 16.27 |

## 3.2. Reactions and Kinetic Model

Dimethyl ether synthesis includes methanol synthesis reactions and dehydration reactions carried out simultaneously. While methanol formation takes place only on CZA catalyst, methanol dehydration occurs either on $\gamma$-$Al_2O_3$ or on HZSM-5 catalyst. In each case, both catalysts are physically mixed with a mass ratio of 1:1 [16, 18, 20]. During these reactions, reverse water gas shift reaction (RWGS) is also carried out implicitly. But, the kinetic expression for RWGS is not stated in order to maintain the independence of the reactions. When $MS_1$, $MS_2$ and MD (shown in the Reaction 2.1, 2.2, 2.3 respectively) reactions are all summed up, as a result, the RWGS reaction is obtained. In order to avoid methane formation reaction stated in the Equation 2.5, the maximum temperature of the reactor should not exceed 573 K [15, 16]. Since the process set to run up to a maximum of 543 K, methane formation is not included in the process kinetics. Another cautious point regarding DME synthesis is that if the reactor temperature is higher than 543 K, CZA catalyst will begin to deactivate due to sintering and coking [15, 16, 20]. Also, by checking the Equation 2.4, $CO_2$ existence prevents coke formation, rxn shifts to the side of CO formation [19].

Corresponding kinetic expressions and the rate parameters are provided in Equations 3.75-3.82 and in Tables 3.6 and 3.7 [15, 16]:

$$R_{\mathrm{MS_1}} = \frac{k_{\mathrm{MS_1}} f_{\mathrm{CO}} f_{\mathrm{H_2}}^2}{(1-\beta_{MS_1})(1+f_{\mathrm{CO}}K_{\mathrm{CO}}+f_{\mathrm{CO_2}}K_{\mathrm{CO_2}}f_{\mathrm{H_2}}K_{\mathrm{H_2}})^3} \; \beta_{MS_1} = \frac{f_{\mathrm{CH_3OH}}}{f_{\mathrm{CO}} f_{\mathrm{H_2}}^2 K_{D,\mathrm{MS_1}}} \quad (3.75)$$

$$R_{\mathrm{MS_2}} = \frac{k_{\mathrm{MS_2}} f_{\mathrm{CO_2}} f_{\mathrm{H_2}}^3 (1-\beta_{MS_2})}{(1+f_{\mathrm{CO}}K_{\mathrm{CO}}+f_{\mathrm{CO_2}}K_{\mathrm{CO_2}}f_{\mathrm{H_2}}K_{\mathrm{H_2}})^4} \qquad \beta_{\mathrm{MS_2}} = \frac{f_{\mathrm{CH_3OH}} f_{\mathrm{H_2O}}}{f_{\mathrm{CO_2}} f_{\mathrm{H_2}}^3 K_{D,\mathrm{MS_2}}} \tag{3.76}$$

$$R_{\mathrm{MD}} = \frac{k_{\mathrm{MD}} f_{\mathrm{CH_3OH}} (1-\beta_{MD})}{(1+\sqrt{K_{\mathrm{CH_3OH}} f_{\mathrm{CH_3OH}}})^2} \qquad \beta_{MD} = \frac{f_{\mathrm{CH_3OCH_3}} f_{\mathrm{H_2O}}}{f_{\mathrm{CH_3OCH_3}}^2 K_{D,\mathrm{MD}}} \tag{3.77}$$

Rate of methanol dehydration in Equation 3.77 was reported for $\gamma$-$Al_2O_3$ catalyst [15]. The rate expression obtained for methanol dehydration on HZSM-5 catalyst is as follows [16]:

$$R_{\mathrm{MD}} = \frac{k_{\mathrm{MD}} (f_{\mathrm{CH_3OH}}^2 - \beta_{MD})}{1+K_{\mathrm{H_2O}} f_{\mathrm{H_2O}} K_{\mathrm{CH_3OH}} f_{\mathrm{CH_3OH}}} \qquad \beta_{MD} = \frac{f_{\mathrm{CH_3OCH_3}} f_{\mathrm{H_2O}}}{K_{D,\mathrm{MD}}} \tag{3.78}$$

Table 3.6. Parameters of the rate constants [15, 16].

| Catalyst | $k_{rxn} = A.\exp^{-E_a/(RT)}$ | A | $E_a$ (J/mol) |
|---|---|---|---|
| CZA | $k_{\mathrm{MS_1}}$ | $1.828 \times 10^3$ | 43723 |
| CZA | $k_{\mathrm{MS_2}}$ | $0.4195 \times 10^2$ | 30253 |
| $\gamma$-$Al_2O_3$ | $k_{\mathrm{MD}}$ | $1.939 \times 10^2$ | 24984 |
| HZSM-5 | $k_{\mathrm{MD}}$ | $1.8966 \times 10^{-3}$ | -4084.1 |

The fugacity required for the rate expressions are calculated as a function of pressure and temperature from the Equation 3.79 [15, 20, 73]:

$$f_i = y_i \qquad f_i = exp\left[\left(b_i - \frac{a_i}{RT}\right)\frac{P}{RT} + lnP\right] \tag{3.79}$$

Partial pressures can be assumed as partial fugacities, hence they are calculated in the use of reaction rate calculations:

$$y_i = \frac{F_i}{F_{tot}} \tag{3.80}$$

$$P_i = f_i \times y_i \tag{3.81}$$

Table 3.7. Adsorption constants for DME formation reactions used in the model [15, 16].

| Catalyst | $K_i = A.\exp^{B/(RT)}$ | A | B (J/mol) |
|---|---|---|---|
| CZA | $K_{CO}$ | $8.252 \times 10^{-4}$ | 30275 |
| CZA | $K_{CO_2}$ | $2.1 \times 10^{-3}$ | 31846 |
| CZA | $K_{H_2}$ | $1.035 \times 10^{-1}$ | -11139 |
| $\gamma$-$Al_2O_3$ | $K_{CH_3OH}$ | $1.726 \times 10^{-4}$ | 60126 |
| HZSM-5 | $K_{CH_3OH}$ | 8.3505 | $3.8867\times10^{-5}$ |
| HZSM-5 | $K_{H_2O}$ | 9.4630 | $1.1274\times10^{-3}$ |

Table 3.8. Van der Waals coefficients for fugacity calculations [73].

| Species ($i$) | $a_i$ | $b_i(\times 10^2)$ |
|---|---|---|
| CO | 1.472 | 3.948 |
| $H_2$ | 0.2453 | 2.651 |
| $CO_2$ | 3.658 | 4.286 |
| $H_2O$ | 5.537 | 3.049 |
| $CH_3OH$ | 9.472 | 6.584 |
| $CH_3OCH_3$ | 8.69 | 7.723 |
| $CH_4$ | 2.3 | 4.301 |

Gibbs free energy of the reactions is calculated from Equations 3.29 and 3.30 stated in the Section 3.1.1.2.

$$K_{eq,rxn} = \frac{exp\,(-\Delta G_{rxn})}{RT} \tag{3.82}$$

where *rxn* stands for $MS_1$, $MS_2$, MD.

# 4. RESULTS AND DISCUSSION

In this present study, the performance of the cascade reactor configuration, which includes adiabatic packed-bed reactors and microchannel heat-exchangers in series, are investigated in the context of a parametric study. For the packed-bed reactors, the effects of feed temperature (473-523 K) and pressure (20-60 bar), the amount and type of catalyst loaded in the packed-bed, and a hypothetical water (steam) removal ratio on CO and $CO_2$ conversions as well as DME yield are studied. For the microchannel heat-exchangers, the role of material and thickness of the wall separating the channels, the type of fluid in the sweep channel are investigated. Discussions of packed-bed reactors and microchannel heat-exchangers are categorized into two subsections so that the influence of each variable can be easily followed.

DME synthesis can be carried out either in a single packed-bed reactor operating isothermally at ca. 523 K or in alternating integrated configurations such as dual-bed membrane reactors or thermally coupled reactors consisting of shell and tubes [10, 15, 20, 42, 49]. The focus of this research is to propose and simulate a reactor system that can provide effective temperature regulation essential for improving DME throughput. As explained previously, temperature regulation is made via the microchannel heat-exchangers inserted between each adiabatic packed-bed. Due to the drastic increase in the temperature along the packed-bed, the length of each bed is kept relatively shorter compared to the isothermal packed-bed reactor [37, 61]. Hence, when the performance of a single bed is investigated, both the syngas conversion and DME yield are relatively lower than those observed in the isothermal case [37, 61]. This drawback is minimized by combining a microchannel heat-exchanger at the end of the adiabatic bed to reduce the temperature, which hence comprises the repeated unit of the cascade reactor configuration.

In the literature, the effectiveness of the bifunctional catalysts is underlined in the direct DME synthesis. In order to validate this statement, simulations are carried out for different physical positions of the methanol synthesis (CZA) and dehydra-

tion ($\gamma$-$Al_2O_3$ or HZSM-5) catalysts. In the mixed-bed case, either CZA+$\gamma$-$Al_2O_3$ or CZA+HZSM-5 catalysts are physically mixed with a mass ratio of 1:1. In the so-called two bed configuration, the simulation is performed with the principle of indirect synthesis of DME meaning that $MS_1$ and $MS_2$ reactions (Reactions 2.1 and 2.2) catalyst (CZA) is loaded in the first bed whereas the MD reaction (Reaction 2.3) catalyst ($\gamma$-$Al_2O_3$ or HZSM-5) is loaded in the consecutive bed. It should be noted that the weight of catalyst used in both configuration are added equally. From the Tables 4.1 and 4.2, for both catalysts, the CO and $CO_2$ conversion almost quadruple in the mixed-bed configuration despite slight rise in the DME yield. To compare the effect of DME formation reaction (MD) catalyst on a single bed, $\gamma$-$Al_2O_3$ performs slightly better than HZSM-5 in terms of syngas conversion whereas worse than HZSM-5 in terms of DME yield.

Table 4.1. Effect of bed configuration on CO conversion, $CO_2$ conversion and DME yield with respect to operating conditions for CZA+$\gamma$-$Al_2O_3$ catalyst for one bed.

| Bed configuration | $w_{cat}$ (kg) | $T_{out}$ (K) | CO conversion (%) | $CO_2$ conversion (%) | DME yield (%) |
|---|---|---|---|---|---|
| Mixed-bed | 0.17 | 544.8 | 6.4 | 4.4 | 2.0 |
| 2 bed conf. | 0.17 | 503.9 | 1.4 | 0.8 | 1.8 |

Table 4.2. Effect of bed configuration on CO conversion, $CO_2$ conversion and DME yield with respect to operating conditions for CZA+HZSM-5 catalyst for one bed.

| Bed configuration | $w_{cat}$ (kg) | $T_{out}$ (K) | CO conversion (%) | $CO_2$ conversion (%) | DME yield (%) |
|---|---|---|---|---|---|
| Mixed-bed | 0.17 | 544.5 | 6.3 | 4.3 | 2.3 |
| 2 bed conf. | 0.17 | 503.9 | 4.5 | 2.9 | 2.0 |

Table 4.3. Inlet flow-rates for cascade packed-bed reactors for CZA+$\gamma$-$Al_2O_3$ catalyst under default conditions (493 K, 50 bar and 0.17 kg catalyst) [15].

| Parameter | Bed 1 | Bed 2 | Bed 3 | Bed 4 | Bed 5 |
|---|---|---|---|---|---|
| $F_{CO}$ (mol/s)($\times 10$) | 1.41 | 1.32 | 1.25 | 1.20 | 1.12 |
| $F_{H_2}$ (mol/s)($\times 10$) | 3.55 | 3.33 | 3.17 | 3.05 | 2.95 |
| $F_{CO_2}$ (mol/s)($\times 10^2$) | 3.36 | 3.22 | 3.13 | 3.09 | 3.06 |
| $F_{H_2O}$ (mol/s)($\times 10^3$) | 1.64 | 1.91 | 3.04 | 3.76 | 4.25 |
| $F_{CH_3OH}$ (mol/s)($\times 10^2$) | 2.46 | 1.21 | 1.90 | 2.42 | 2.86 |
| $F_{DME}$ (mol/s)($\times 10^3$) | 1.48 | 1.78 | 2.08 | 2.37 | 2.63 |
| $F_{CH_4}$ (mol/s)($\times 10^2$) | 3.61 | 3.61 | 3.61 | 3.61 | 3.61 |
| $F_{N_2}$ (mol/s)($\times 10$) | 2.51 | 2.51 | 2.51 | 2.51 | 2.51 |
| Total flow-rate (mol/s)($\times 10$) | 8.22 | 8.01 | 7.86 | 7.74 | 7.65 |

Table 4.4. Inlet flow-rates for cascade packed-bed reactors for CZA+HZSM-5 catalyst under default conditions (493 K, 50 bar and 0.17 kg catalyst) [15].

| Parameter | Bed 1 | Bed 2 | Bed 3 |
|---|---|---|---|
| $F_{CO}$ (mol/s)($\times 10$) | 1.41 | 1.32 | 1.24 |
| $F_{H_2}$ (mol/s)($\times 10$) | 3.55 | 3.33 | 3.15 |
| $F_{CO_2}$ (mol/s)($\times 10^2$) | 3.36 | 3.21 | 3.14 |
| $F_{H_2O}$ (mol/s)($\times 10^3$) | 1.64 | 2.12 | 4.88 |
| $F_{CH_3OH}$ (mol/s)($\times 10^2$) | 2.46 | 1.20 | 2.38 |
| $F_{DME}$ (mol/s)($\times 10^3$) | 1.48 | 1.98 | 4.03 |
| $F_{CH_4}$ (mol/s)($\times 10^2$) | 3.61 | 3.61 | 3.61 |
| $F_{N_2}$ (mol/s)($\times 10$) | 2.51 | 2.51 | 2.51 |
| Total flow-rate (mol/s)($\times 10$) | 8.22 | 8.01 | 7.83 |

## 4.1. Parametric Study on Adiabatic Packed-Bed Reactors in Cascade Reactor System

In this section, the effects of inlet temperature and pressure to the packed-beds and the amount of catalyst used in the reactors on temperature distribution, carbon oxide conversions and DME yield are studied. In these studies pressure drop along the packed-beds are not taken into account. Nevertheless, pressure drop as a constraint on the design of the cascade system will be discussed in Section 4.3.

### 4.1.1. Effect of Inlet Temperature

The changes in syngas conversion, DME yield, maximum attainable number of bed and the amount of catalyst required to carry out the DME synthesis reactions are investigated by varying inlet temperature from 473 to 523 K. The determination of maximum attainable bed number is dependent upon two restrictions when the pressure drop is not taken into consideration: $CO_2$ conversion should not drop below zero for each bed, and the maximum reactor temperature should not exceed 543 K due to catalyst sintering. Both restrictions are negatively affected by the increase in the catalyst weight loaded in the packed-bed reactors. The second limitation is especially important in the first bed of the system because it plays a significant role in determining the maximum amount of catalyst weight loaded in each consecutive packed-beds under different conditions. As bed number increases along with the system, at some point, $CO_2$ conversion converges to negative values for a given catalyst weight. In that way, the determination of the maximum attainable bed number is achieved. While the inlet temperature varies by increasing 5 K in each case, the other parameters are kept under default conditions stated in Section 4.1.

The comparison of inlet temperature is illustrated for a single packed-bed and multi-bed configuration for both CZA+$\gamma$-$Al_2O_3$ and CZA+HZSM-5 bifuncitonal catalysts. The lower the inlet temperature, the higher required the weight of the catalyst. For example, when the inlet temperature is at 473.2 K, 0.63 kg CZA+$\gamma$-$Al_2O_3$ catalyst and 0.62 CZA+HZSM-5 catalyst should be loaded to a single bed for obtaining the

maximum reactor outlet temperature of 543.2 K. These amounts are three times higher than the catalyst weight needed when feeding at 493.2 K.

Table 4.5. Effect of inlet temperature on CO conversion, $CO_2$ conversion and DME yield with respect to operating conditions for CZA+$\gamma$-$Al_2O_3$ catalyst for one bed.

| Case number | $T_{in}$ (K) | $w_{cat}$ (kg) | $T_{out}$ (K) | CO conversion (%) | $CO_2$ conversion (%) | DME yield (%) |
|---|---|---|---|---|---|---|
| 1 | 473.2 | 0.63 | 542.9 | 8.7 | 5.3 | 2.35 |
| 2 | 478.2 | 0.45 | 543.7 | 8.1 | 5.1 | 2.26 |
| 3 | 483.2 | 0.33 | 543.3 | 7.5 | 4.8 | 2.18 |
| 4 | 488.2 | 0.24 | 542.8 | 6.8 | 4.5 | 2.10 |
| 5 | 493.2 | 0.17 | 544.9 | 6.4 | 4.4 | 2.05 |
| 6 | 498.2 | 0.12 | 543.1 | 5.6 | 3.9 | 1.98 |
| 7 | 503.2 | 0.090 | 543.3 | 5.0 | 3.6 | 1.93 |
| 8 | 508.2 | 0.065 | 543.4 | 4.4 | 3.2 | 1.89 |
| 9 | 513.2 | 0.046 | 542.8 | 3.7 | 2.8 | 1.85 |

For the multiple bed configuration in CZA+$\gamma$-$Al_2O_3$ case, despite the significant difference in the catalyst amount loaded in the bed and the same maximum attainable bed number, the difference in the $CO_2$ conversion and DME yield are not significant. Due to greater catalyst amount, CO conversion reaches around 26% at the inlet temperature 473.2 K and 22% at the inlet temperature 493.2 K. On the other hand, when the inlet temperature exceeds 498.2 K, in order to keep the outlet temperature below the limit, 543.2 K, much less amount of catalyst should be loaded into the packed-beds. In that case, despite the temperature rise, all of the variables are inversely affected. Although the maximum attainable bed number increases in both CZA+$\gamma$-$Al_2O_3$ and CZA+HZSM-5 cases for the inlet temperatures of 508.2 and 513.2 K, CO conversion, in particular, decreases approximately 20 in CZA+$\gamma$-$Al_2O_3$ case compared to the 493.2 K. This fact can be associated with the significant decrease in catalyst weight loaded in each bed. With the given feed composition stated in Tables 4.3 and 4.4, CO conversion

($MS_2$ (Reaction 2.1)) is unaffected by the DME formation reaction, which results in a certain amount of water formation. Hence, the more catalyst weight refers to the more CO conversion. Also, the similar pattern can be observed in $CO_2$ conversion and DME yield due to fewer catalyst weight. The results of multiple bed configuration for CZA+$\gamma$-$Al_2O_3$ and CZA+HZSM-5 catalysts are found in the Tables 4.7 and 4.8 respectively.

Table 4.6. Effect of inlet temperature on CO conversion, $CO_2$ conversion and DME yield with respect to operating conditions for CZA+HZSM-5 catalyst for one bed.

| Case number | $T_{in}$ (K) | $w_{cat}$ (kg) | $T_{out}$ (K) | CO conversion (%) | $CO_2$ conversion (%) | DME yield (%) |
|---|---|---|---|---|---|---|
| 1 | 473.2 | 0.62 | 542.9 | 8.7 | 5.1 | 3.4 |
| 2 | 478.2 | 0.45 | 542.8 | 8.3 | 5.0 | 3.1 |
| 3 | 483.2 | 0.33 | 543.7 | 7.7 | 4.9 | 2.8 |
| 4 | 488.2 | 0.23 | 543.0 | 6.4 | 4.2 | 2.4 |
| 5 | 493.2 | 0.17 | 543.1 | 6.3 | 4.3 | 2.3 |
| 6 | 498.2 | 0.13 | 543.3 | 5.8 | 4.1 | 2.1 |
| 7 | 503.2 | 0.091 | 543.9 | 5.2 | 3.7 | 2.0 |
| 8 | 508.2 | 0.065 | 534.8 | 4.5 | 3.3 | 1.9 |
| 9 | 513.2 | 0.047 | 543.9 | 3.8 | 2.9 | 1.8 |

In CZA+HZSM-5 case, on the other hand, the maximum attainable bed numbers are significantly lesser than that of the CZA+$\gamma$-$Al_2O_3$ case. The main reason for this significant drop is associated with the much higher MD reaction rate referring to higher methanol decomposition and, in turn, much water formation. Due to increased water amount in the reactor, a shift to RWGS (Reaction 2.4) reaction is observed, which results in the decrease in $CO_2$ conversion below the limitations at some point of the reactor length. Apart from the bed number, the effect of inlet temperature on the syngas conversions is similar to CZA+$\gamma$-$Al_2O_3$ case.

The most striking difference between CZA+$\gamma$-$Al_2O_3$ and CZA+HZSM-5 cases can be seen in the DME yield results. Despite fewer consecutive bed numbers, the DME yield of CZA+HZSM-5 is higher than two times of the CZA+$\gamma$-$Al_2O_3$ case.

Table 4.7. Effect of inlet temperature on CO conversion, $CO_2$ conversion and DME yield with respect to operating conditions for CZA+$\gamma$-$Al_2O_3$ catalyst.

| Case number | Maximum bed number | $T_{in}$ (K) | $w_{cat}$ (kg) | CO conversion (%) | $CO_2$ conversion (%) | DME yield (%) |
|---|---|---|---|---|---|---|
| 1 | 5 | 473.2 | 0.63 | 26.0 | 10.2 | 5.63 |
| 2 | 5 | 478.2 | 0.45 | 23.0 | 9.9 | 3.91 |
| 3 | 5 | 483.2 | 0.33 | 23.9 | 9.7 | 3.87 |
| 4 | 5 | 488.2 | 0.24 | 22.6 | 9.5 | 3.57 |
| 5 | 5 | 493.2 | 0.17 | 21.6 | 9.2 | 3.34 |
| 6 | 5 | 498.2 | 0.12 | 19.8 | 9.1 | 3.08 |
| 7 | 5 | 503.2 | 0.090 | 18.3 | 8.9 | 2.87 |
| 8 | 6 | 508.2 | 0.065 | 18.9 | 8.7 | 2.86 |
| 9 | 6 | 513.2 | 0.046 | 16.7 | 8.6 | 2.64 |

Overall, if the same weight of catalyst is inserted in the cases for different inlet temperatures, the optimum inlet temperatures compared with the weight of catalyst can be determined in the range of 488-498 K from the Tables 4.5-4.8. To compare the performance of the catalysts, CZA+$\gamma$-$Al_2O_3$ allows more maximum attainable bed number, but even with higher bed number, it can not outweigh the outcomes of CZA+HZSM-5 catalyst in terms of DME yield.

Table 4.8. Effect of inlet temperature on CO conversion, $CO_2$ conversion and DME yield with respect to operating conditions for CZA+HZSM-5 catalyst.

| Case number | Maximum bed number | $T_{in}$ (K) | $w_{cat}$ (kg) | CO conversion (%) | $CO_2$ conversion (%) | DME yield (%) |
|---|---|---|---|---|---|---|
| 1 | 1 | 473.2 | 0.62 | 8.7 | 5.1 | 3.4 |
| 2 | 1 | 478.2 | 0.45 | 8.3 | 5.0 | 3.1 |
| 3 | 1 | 483.2 | 0.32 | 7.7 | 4.9 | 2.8 |
| 4 | 3 | 488.2 | 0.23 | 13.1 | 6.4 | 5.4 |
| 5 | 3 | 493.2 | 0.17 | 17.2 | 6.7 | 8.1 |
| 6 | 3 | 498.2 | 0.13 | 15.4 | 7.1 | 6.5 |
| 7 | 3 | 503.2 | 0.091 | 13.6 | 7.2 | 5.1 |
| 8 | 4 | 508.2 | 0.065 | 14.7 | 7.4 | 5.4 |
| 9 | 5 | 513.2 | 0.047 | 15.6 | 7.4 | 5.5 |

### 4.1.2. Effect of Weight of Catalyst

The dependence of CO and $CO_2$ conversions as well as DME yield on the catalyst weight are investigated in this section. For this purpose, inlet temperature and pressure to packed-beds are fixed to 493.2 K and 50 bar, respectively. Inlet molar flow-rates of the species are specified in Tables 4.3 and 4.4. The dependence of CO and $CO_2$ conversions as well as DME yield on the catalyst weight are investigated in this section. The change in maximum bed attainable number is also tabulated in Tables 4.11 and 4.12 CZA+$\gamma$-$Al_2O_3$ and CZA+HZSM-5 catalysts respectively. In Chapter 3, it is stated that above 543.2 K, the deactivation of the CZA catalyst due to combined sintering and coke formation is likely to occur. However, during this study, catalyst deactivation is omitted by limiting the maximum bed temperature to 543.2 K in all cases. Also, methane formation is neglected as it becomes significant only above around 573.2 K [15, 19].

Table 4.9. Effect of weight of catalyst on CO conversion, $CO_2$ conversion and DME yield with respect to operating conditions for CZA+$\gamma$-$Al_2O_3$ catalyst for one bed.

| Case number | $w_{cat}$ (kg) | $T_{out}$ (K) | CO conversion (%) | $CO_2$ conversion (%) | DME yield (%) |
|---|---|---|---|---|---|
| 1 | 0.15 | 523.3 | 3.8 | 2.5 | 1.93 |
| 2 | 0.16 | 528.4 | 2.9 | 4.4 | 1.96 |
| 3 | 0.16 | 533.2 | 3.3 | 5.0 | 1.99 |
| 4 | 0.17 | 538.4 | 3.8 | 5.6 | 2.13 |
| 5 | 0.17 | 544.9 | 4.4 | 6.4 | 2.05 |
| 6 | 0.17 | 547.9 | 4.7 | 6.8 | 2.06 |
| 7 | 0.18 | 553.0 | 5.1 | 7.4 | 2.09 |
| 8 | 0.18 | 558.5 | 5.5 | 8.1 | 2.12 |
| 9 | 0.18 | 561.0 | 5.9 | 8.8 | 2.16 |

Intuitively, the more catalyst loaded in the bed, the faster the reactions takes place. When single bed configuration for both CZA+$\gamma$-$Al_2O_3$ and CZA+HZSM-5 are observed from the Tables 4.9 and 4.10, it can bee seen that the syngas conversion has increased more than 50 %. The increase in the DME yield, on the other hand, is not that extreme due to $MS_2$ reaction (Reaction 2.2). As $MS_2$ reaction is carried out, water arises as a by-product. Hence, MD reaction tends to shift to the direction of methanol formation, meaning that the produced DME is started to be converted.

In the case of multi-bed configuration, as the weight of catalyst in each bed increases, the maximum attainable bed number decreases for both catalyst types. This fact can be explained as follows: An increase in the catalyst amount in the bed leads to an increase in the syngas conversion and DME formation. During these reactions, as mentioned earlier, the water amount rises to some extent from the Reactions 2.2 and 2.3. The formation of the water, in turn, hampers $CO_2$ conversion and stimulates $CO_2$ formation instead. The computation of the code stops automatically when $CO_2$ conversion becomes negative.

Table 4.10. Effect of weight of catalyst on CO conversion, $CO_2$ conversion and DME yield with respect to operating conditions for CZA+HZSM-5 catalyst for one bed.

| Case number | $w_{cat}$ (kg) | $T_{out}$ (K) | CO conversion (%) | $CO_2$ conversion (%) | DME yield (%) |
|---|---|---|---|---|---|
| 1 | 0.15 | 523.3 | 3.9 | 2.5 | 2.07 |
| 2 | 0.16 | 528.3 | 3.9 | 2.9 | 2.12 |
| 3 | 0.16 | 533.1 | 5.1 | 3.4 | 2.18 |
| 4 | 0.17 | 538.1 | 5.7 | 3.8 | 2.23 |
| 5 | 0.17 | 543.1 | 6.3 | 4.3 | 2.28 |
| 6 | 0.17 | 548.7 | 6.9 | 4.7 | 2.31 |
| 7 | 0.18 | 553.3 | 7.5 | 5.1 | 2.36 |
| 8 | 0.18 | 558.7 | 8.0 | 5.4 | 2.39 |
| 9 | 0.18 | 563.1 | 8.7 | 5.7 | 2.45 |

Table 4.11. Effect of weight of catalyst on CO conversion, $CO_2$ conversion and DME yield with respect to operating conditions for CZA+$\gamma$-$Al_2O_3$ catalyst.

| Case number | Maximum bed number | $w_{cat}$ (kg) | CO conversion (%) | $CO_2$ conversion (%) | DME yield (%) |
|---|---|---|---|---|---|
| 1 | 8 | 0.15 | 22.9 | 9.50 | 3.65 |
| 2 | 7 | 0.16 | 22.7 | 9.43 | 3.57 |
| 3 | 6 | 0.16 | 21.8 | 9.37 | 3.43 |
| 4 | 5 | 0.17 | 20.4 | 9.28 | 3.25 |
| 5 | 5 | 0.17 | 21.6 | 9.22 | 3.34 |
| 6 | 5 | 0.17 | 22.1 | 9.18 | 3.38 |
| 7 | 4 | 0.18 | 20.0 | 9.10 | 3.13 |
| 8 | 4 | 0.18 | 20.8 | 9.05 | 3.19 |
| 9 | 4 | 0.18 | 21.5 | 8.92 | 3.25 |

To sum up, water formation in these reactions results in a tradeoff between $CO_2$ conversion and DME yield. This effect can be specifically observed within case 7-9 for both CZA+$\gamma$-$Al_2O_3$ and CZA+HZSM-5 catalyst configurations. The turning point for the DME yield can be seen in case 7 and 6 for CZA+$\gamma$-$Al_2O_3$ and CZA+HZSM-5, respectively. The CO conversion is not affected by this phenomenon, hence, it continues rising proportionally to the weight of catalyst loaded in the bed.

Table 4.12. Effect of weight of catalyst on CO conversion, $CO_2$ conversion and DME yield with respect to operating conditions for CZA+HZSM-5 catalyst.

| Case number | Maximum bed number | $w_{cat}$ (kg) | CO conversion (%) | $CO_2$ conversion (%) | DME yield (%) |
|---|---|---|---|---|---|
| 1 | 5 | 0.15 | 17.9 | 7.7 | 10.2 |
| 2 | 4 | 0.16 | 16.6 | 7.5 | 8.8 |
| 3 | 4 | 0.16 | 18.4 | 7.2 | 9.8 |
| 4 | 3 | 0.17 | 16.0 | 7.0 | 7.5 |
| 5 | 3 | 0.17 | 17.2 | 6.7 | 8.1 |
| 6 | 2 | 0.18 | 13.2 | 6.6 | 5.0 |
| 7 | 2 | 0.18 | 14.2 | 6.3 | 5.3 |
| 8 | 2 | 0.18 | 14.8 | 6.1 | 5.6 |
| 9 | 1 | 0.18 | 8.7 | 5.7 | 2.4 |

It should be noted that despite the limited number of packed bed in the ones loaded with more weight of the catalyst, the CO, $CO_2$ conversion and DME yield values are within the range of 22.9-20.0, 9.5-8.9, and 3.65-3.2 respectively for CZA+$\gamma$-$Al_2O_3$ catalyst, and 18.4- 13.2, 7.7-5.7, and 10.2-2.4 respectively for CZA+HZSM-5 catalyst. These results seem to illustrate the fact that CZA+$\gamma$-$Al_2O_3$ removes more syngas compared to CZA+HZSM-5 whereas CZA+HZSM-5 outweighs CZA+$\gamma$-$Al_2O_3$ in terms of DME yield. The first part of the statement can be misleading because in the configuration of CZA+$\gamma$-$Al_2O_3$ catalyst, the maximum attainable bed number is higher than CZA+HZSM-5 for all cases due to the $CO_2$ conversion restriction.

From these results, case 5 is determined as the optimum point for $CO_2$ conversion, DME yield and catalyst amount for both catalysts.

### 4.1.3. Effect of Feed Inlet Pressure

In this subsection, the investigation of the syngas conversion and DME yield with respect to pressure change is performed in the range of 20-60 bar for CZA+$\gamma$-$Al_2O_3$ and CZA+HZSM-5 catalyst configurations. During these studies, the inlet temperature and catalyst weight per bed are taken as 493.2 K and 0.17 kg, respectively. Feed conditions are taken as presented in Tables 4.3 and 4.4. Similar to the other parametric studies, the pressure drop along the reactor is omitted.

Table 4.13. Effect of pressure on CO conversion, $CO_2$ conversion and DME yield with respect to operating conditions for CZA+$\gamma$-$Al_2O_3$ catalyst for one bed.

| Case number | $P_{in}$ (bar) | $w_{cat}$ (kg) | $T_{out}$ (K) | CO conversion (%) | $CO_2$ conversion (%) | DME yield (%) |
|---|---|---|---|---|---|---|
| 1 | 20 | 0.17 | 512.3 | 2.4 | 1.4 | 1.91 |
| 2 | 20 | 0.30 | 537.5 | 5.6 | 2.6 | 2.34 |
| 3 | 30 | 0.17 | 521.1 | 3.5 | 2.2 | 1.95 |
| 4 | 30 | 0.23 | 542.7 | 6.3 | 3.3 | 2.19 |
| 5 | 40 | 0.17 | 531.1 | 4.7 | 3.1 | 2.01 |
| 6 | 40 | 0.19 | 543.4 | 6.2 | 4.1 | 2.07 |
| 7 | 50 | 0.17 | 544.9 | 6.4 | 4.4 | 2.05 |
| 8 | 60 | 0.17 | 569.0 | 9.3 | 6.6 | 2.14 |
| 9 | 60 | 0.16 | 543.5 | 6.2 | 4.3 | 2.02 |

Due to Le Chatelier's principle, both methanol synthesis reactions (Reactions 2.1 and 2.2) shift to the direction of methanol formation upon increase in pressure. However, since methanol dehydration (Reactions 2.3) is stoichiometrically equal in the reactant and product sides, it is not stimulated by pressure rise. Therefore, an increase

in pressure leads to more methanol formation and more methanol conversion in the methanol dehydration.

Table 4.14. Effect of pressure on CO conversion, $CO_2$ conversion and DME yield with respect to operating conditions for CZA+HZSM-5 catalyst for one bed.

| Case number | $P_{in}$ (bar) | $w_{cat}$ (kg) | $T_{out}$ (K) | CO conversion (%) | $CO_2$ conversion (%) | DME yield (%) |
|---|---|---|---|---|---|---|
| 1 | 20 | 0.17 | 511.8 | 2.4 | 1.4 | 1.77 |
| 2 | 20 | 0.30 | 536.9 | 5.5 | 2.9 | 2.01 |
| 3 | 30 | 0.17 | 520.4 | 3.5 | 2.2 | 1.89 |
| 4 | 30 | 0.22 | 544.6 | 5.1 | 3.3 | 2.00 |
| 5 | 40 | 0.17 | 531.1 | 4.7 | 3.1 | 2.06 |
| 6 | 40 | 0.19 | 545 | 6.4 | 3.9 | 2.10 |
| 7 | 50 | 0.17 | 544.6 | 6.3 | 4.3 | 2.28 |
| 8 | 60 | 0.17 | 572.7 | 9.8 | 6.5 | 2.61 |
| 9 | 60 | 0.16 | 543.7 | 6.2 | 4.3 | 2.36 |

It can be seen from the Tables 4.13 and 4.14, for each pressure, except for 50 bar, the results are tabulated for two cases for each pressure tested. In the first cases, the default amount of catalyst (0.17 kg) is loaded in the packed-bed. In the second cases, the amount of catalyst weight is adjusted such that maximum allowable temperature of 543.2 K is reached. An exception is observed for case 9 since the pressure promotes syngas conversion, the exothermicity of the methanol formation reactions leads to a significant temperature rise at 60 bar. Hence, for this case, the catalyst weight is adjusted for not exceeding the maximum allowable temperature, 543.2 K. At the same catalyst amount, the syngas conversion approximately triples the value of 20 bar at 60 bar. For one bed configuration, CZA+HZSM-5 performs slightly better than CZA+$\gamma$-$Al_2O_3$ catalyst in terms of syngas conversion and DME yield above 40 bar.

The multi-packed-bed configurations are tabulated in Tables 4.15 and 4.16. Despite the same amount of catalyst loaded in each bed mostly, CZA+$\gamma$-$Al_2O_3$ enables more maximum attainable bed number in all cases compared to CZA+HZSM-5. When the molar flow-rate of water, methanol and DME are checked from the Tables 4.3 and 4.4, methanol dehydration reaction occurs in CZA+$\gamma$-$Al_2O_3$ slightly faster than CZA+HZSM-5 catalyst in the first three packed-bed. At the end of bed 3, though, CZA+HZSM-5 performs way better than CZA+$\gamma$-$Al_2O_3$ in terms of DME synthesis, which results in more water and DME. However, it should be reminded that more water formation leads to hampering the $CO_2$ conversion due to the RWGS. Hence, $CO_2$ conversion becomes negative at the end of bed-3 for case 7 for CZA+HZSM-5. On the other hand, despite the lower number of maximum attainable beds, by using CZA+HZSM-5 catalyst, CO and $CO_2$ conversions are comparable with CZA+$\gamma$-$Al_2O_3$ in cases 1, 4, 7. The DME yield for CZA+HZSM-5 is higher than CZA+$\gamma$-$Al_2O_3$ except case 2.

Table 4.15. Effect of pressure on CO conversion, $CO_2$ conversion and DME yield with respect to operating conditions for CZA+$\gamma$-$Al_2O_3$ catalyst.

| Case number | Maximum bed number | $P_{in}$ (bar) | CO conversion (%) | $CO_2$ conversion (%) | DME yield (%) |
|---|---|---|---|---|---|
| 1 | 5 | 20 | 9.6 | 3.6 | 2.8 |
| 2 | 2 | 20 | 9.3 | 2.6 | 2.9 |
| 3 | 7 | 30 | 19.6 | 7.8 | 3.5 |
| 4 | 3 | 30 | 13.6 | 5.2 | 2.9 |
| 5 | 5 | 40 | 17.6 | 7.5 | 3.2 |
| 6 | 4 | 40 | 17.4 | 7.3 | 3.1 |
| 7 | 5 | 50 | 21.6 | 9.2 | 3.3 |
| 8 | 5 | 60 | 26.2 | 10.8 | 3.5 |
| 9 | 6 | 60 | 25.3 | 11.1 | 3.6 |

Table 4.16. Effect of pressure on CO conversion, $CO_2$ conversion and DME yield with respect to operating conditions for CZA+HZSM-5 catalyst.

| Case number | Maximum bed number | $P_{in}$ (bar) | CO conversion (%) | $CO_2$ conversion (%) | DME yield (%) |
|---|---|---|---|---|---|
| 1 | 4 | 20 | 8.1 | 3.5 | 3.0 |
| 2 | 1 | 20 | 5.5 | 2.9 | 2.0 |
| 3 | 4 | 30 | 12.0 | 4.8 | 5.2 |
| 4 | 2 | 30 | 10.9 | 4.4 | 3.8 |
| 5 | 3 | 40 | 12.9 | 6.0 | 5.6 |
| 6 | 2 | 40 | 11.7 | 5.5 | 4.2 |
| 7 | 3 | 50 | 17.2 | 6.7 | 8.1 |
| 8 | 1 | 60 | 9.8 | 6.5 | 2.6 |
| 9 | 3 | 60 | 18.5 | 7.8 | 9.0 |

From these results, it is clear that the pressure increase results in the stimulation of methanol formation due to Le Chatelier's principle, which, in turn, has a positive effect on the syngas conversion as well as the DME yield. Hence, higher pressure is more preferable for the operating conditions with economic considerations.

## 4.2. Effect of Water Removal in Cascade Reactor System

Water formation in the DME synthesis is an undesirable phenomenon which particularly hinders the $CO_2$ conversion due to RWGS as (Reaction 2.4). For this reason, in this section, a hypothetical study is conducted based on water removal from each packed-bed outlet. The studies are carried out under default conditions, namely 493.2 K, 50 bar, 0.17 kg catalyst and the feed conditions reported in Tables 4.3 and 4.4. Since the maximum outlet temperature value varies with respect to the inlet temperature, pressure or catalyst amount, the outlet temperatures for water removal cases are not presented in the results given in this section. In addition, the effect of water removal is investigated only for CZA+HZSM-5 catalyst configuration because

CZA+HZSM-5 performs close results for CO and $CO_2$ conversions and slightly higher results for the DME yield with less bed number compared to CZA+$\gamma$-$Al_2O_3$.

Table 4.17 shows the results obtained under the default conditions when no $CO_2$ conversions, and DME yield are presented in Tables 4.18 - 4.20, respectively. Several strategies are tested for better understanding of the water removal effect. In the stage-wise water removal, at the exit of packed-bed 1, the water removal is 30%, and in the following beds, the ratio is incremented by 5 consecutively. In the third case, at the exit of the first three packed-bed, the water release ratio is taken as 30% whereas the consecutive two beds experience 50% of the water removal. The forth case is similar to case 4 but varies in terms of the order of water removal ratio. Instead of applying 30% water ratio beds at the beginning, 50% separation of water removal is applied.

Table 4.17. The CO conversion, $CO_2$ conversion and DME yield under default conditions for CZA+HZSM-5 catalyst.

| Maximum bed number | $w_{cat}$ (bar) | CO conversion (%) | $CO_2$ conversion (%) | DME yield (%) |
|---|---|---|---|---|
| 3 | 0.17 | 17.2 | 6.7 | 8.1 |

The CO conversion is the highest at case 4, 29.6 % and other combinations also provide closer CO conversion above 29%. For the $2^{nd}$, $3^{rd}$ , and $4^{th}$ bed, the variation in the ratio of water removal seems insignificant. The slight variations for CO conversion for different water removal ratios can be seen especially after the exit of $4^{th}$ bed. Nevertheless, the change in CO conversion is less than 1% at the exit of the bed 6. However, due to higher amount of water formation, even 30% water removal is not enough to increase the maximum attainable bed number. Finally, when the results are compared with the default case, for bed 3, the effect of water removal percentage on CO conversion is negligible.

Overall, the order of water ratio slightly affects the CO conversion. The increase in water ratio, for sure, influences the system compared to the default case in which

no water is removed from the system. However, the results obtained from this study illustrates that the enhancement of the required parameters is not as significant as the change in the water removal ratio from 30 to 50%. This fact is consistent with Le Chatelier's principle because the methanol formation reaction, (Reaction 2.1), is not affected by the presence of the water.

Table 4.18. Effect of water removal percentage on CO conversion for CZA+HZSM-5 catalyst.

| Number of bed | 30 % water removal | Stage-wise % water removal | First 2 30 % then last 3 50 % | First 3 50 % then last 2 30 % |
|---|---|---|---|---|
| 1 | 6.3 | 6.3 | 6.3 | 6.3 |
| 2 | 12.4 | 12.4 | 12.4 | 12.5 |
| 3 | 17.6 | 17.7 | 17.6 | 17.9 |
| 4 | - | 22.0 | 22.1 | 22.4 |
| 5 | - | 25.9 | 26.0 | 26.2 |
| 6 | - | 29.4 | 29.5 | 29.6 |

Table 4.19. Effect of water removal percentage on $CO_2$ conversion for CZA+HZSM-5 catalyst.

| Number of bed | 30 % water removal | Stage-wise % water removal | First 2 30 % then last 3 50 % | First 3 50 % then last 2 30 % |
|---|---|---|---|---|
| 1 | 4.3 | 4.3 | 4.3 | 4.3 |
| 2 | 6.9 | 6.9 | 6.9 | 7.1 |
| 3 | 7.5 | 7.6 | 7.5 | 8.1 |
| 4 | - | 7.8 | 7.9 | 8.5 |
| 5 | - | 8.1 | 8.4 | 8.6 |
| 6 | - | 8.7 | 9.0 | 8.6 |

As opposed to CO conversion, water removal influences $CO_2$ conversion to some extent. The change of order of water removal ratio slightly improves the $CO_2$ conversion at the end of the bed-6 by checking case 3 and 4. The highest $CO_2$ conversion (9.0%) is obtained in the case 4 whereas the lowest $CO_2$ conversion remains at 7.5% for the 30% water removal case at bed 3. For the other cases, the $CO_2$ conversion is found in the range of 9.0 - 8.6%. The variation in the $CO_2$ conversion can be observed starting from the exit of bed-2 from Table 4.19.

To sum up, the ratio of water removal influences more than the heat-exchangers' position possessing higher or lower water removal ratio to $CO_2$ conversion in the cascade bed configuration. The water removal delivers a significantly higher maximum attainable number of beds than the default case since the water removal stimulates $CO_2$ conversion, and the computation stops in the compiler until when $CO_2$ conversion becomes negative with no pressure drop. The less water in the system tends to the less shift of water to RWGS reaction.

Table 4.20. Effect of water removal percentage on DME yield for CZA+HZSM-5 catalyst.

| Number of bed | 30 % water removal | Stage-wise % water removal | First 2 30 % then last 3 50 % | First 3 50 % then last 2 30 % |
|---|---|---|---|---|
| 1 | 2.3 | 2.3 | 2.3 | 2.3 |
| 2 | 4.7 | 4.7 | 4.7 | 4.8 |
| 3 | 8.3 | 8.4 | 8.4 | 8.5 |
| 4 | - | 12.3 | 12.3 | 12.6 |
| 5 | - | 16.1 | 16.2 | 16.4 |
| 6 | - | 19.6 | 19.7 | 19.8 |

The trend in the rise of DME yield is similar to that of CO conversion with water removal. The negligible variations in DME yield can be observed at the exit of bed-3. DME yield is increased from 8.1 to 8.5% compared to the default case for

CZA+HZSM-5 catalyst at the exit of bed-3. At the end of the bed-6, there are no significant changes in the DME yield for Case 2 to 4.

### 4.3. Design of Adiabatic Packed-Bed Reactors in Cascade Reactor System

Up to this section, the effect of inlet temperature, pressure as well as the catalyst amount is calculated without the consideration of pressure drop. In this section, on the other hand, the dimensions of the packed-bed reactor are precisely determined including pressure drop effect. The determination of the dimensions is explained elaborately in the Section of 3.1.1. As the CZA+$\gamma$-$Al_2O_3$ and CZA+HZSM-5 catalysts mixtures have different bulk density values (1273 and 1200 kg/m$^3$ respectively [15,18,61].), the length of the packed-bed reactor for each catalyst type varies under the same inner diameter of 0.025 m [15, 18, 61]. For CZA+HZSM-5 and CZA+$\gamma$-$Al_2O_3$, the reactor length is estimated at 0.29 and 0.28 m respectively. For both cases, the aspect ratio (L/D) is maintained above 10 for providing the plug flow assumption [31].

Table 4.21. Pressure drop along the packed-beds loaded with CZA+$\gamma$-$Al_2O_3$ catalyst under default conditions (493 K, 50 bar and 0.17 kg catalyst).

| Bed | $P_{in}$ (Bar) | $P_{out}$ (Bar) | Pressure drop (%) |
|---|---|---|---|
| 1 | 50.0 | 49.1 | 1.8 |
| 2 | 49.1 | 48.5 | 1.4 |
| 3 | 48.5 | 47.7 | 1.6 |
| 4 | 47.7 | 46.9 | 1.7 |
| 5 | 46.9 | 46.1 | 1.7 |
| Overall | 6.2 | | |

The maximum attainable bed number for CZA+$\gamma$-$Al_2O_3$ and CZA+HZSM-5 catalyst is stated as 5 and 3 respectively previously. When pressure drop along the bed is taken into account, the pressure drop per each bed is limited to 2.5%. Hence, the overall pressure drop is maintained below 10% in the cascade reactor configuration. Despite higher bed number, the maximum allowable bed number for CZA+$\gamma$-$Al_2O_3$ is

attained to 5. The pressure drop with respect to bed number is tabulated as in Tables 4.21 and 4.22 :

Table 4.22. Pressure drop along the packed-beds loaded with CZA+HZSM-5 catalyst under default conditions (493 K, 50 bar and 0.17 kg catalyst).

| Bed | $P_{in}$ (Bar) | $P_{out}$ (Bar) | Pressure drop (%) |
|---|---|---|---|
| 1 | 50.00 | 48.91 | 2.19 |
| 2 | 48.91 | 47.79 | 2.28 |
| 3 | 47.79 | 46.65 | 2.38 |
| Overall | 6.70 | | |

Due to the smaller length of the CZA+$\gamma$-$Al_2O_3$ configuration, the overall pressure drop % is slightly less than CZA+HZSM-5 catalyst configuration. In both cases, the pressure drop values are consistent with the criteria of maximum 2.5 % pressure drop per bed. Other parameters affecting the pressure drop in the packed-bed reactors are the particle diameter of catalyst and bed porosity [31]. According to De Falco *et al.* [61] and Vakili *et al.* [18], the particle diameter of CZA+$\gamma$-$Al_2O_3$ and CZA+HZSM-5 catalysts are 0.005 and 0.002 m, respectively. From Ergun's equation (Equation 3.41), the more the particle diameter, the less pressure drop along the packed-bed.Since CZA+$\gamma$-$Al_2O_3$ catalyst's particle diameter is approximately three times greater than that of CZA-HSZM-5 catalyst has, the overall pressure drop in CZA+$\gamma$-$Al_2O_3$ case is lesser than that of the CZA-HSZM-5. When bed porosity is taken into account, since bed porosity is taken as 0.39 for both catalysts, the effect of bed porosity on the pressure drop is almost the same for both catalysts. The outlet flow-rates for each bed are tabulated of species from both catalyst types. Since methane formation is omitted and $N_2$ is inserted to the system as inert, the molar flow-rates of $CH_4$ and $N_2$ remain constant in all beds.

Table 4.23. Outlet flow-rates (mol.s$^{-1}$) for cascade packed-bed reactors for CZA+$\gamma$-$Al_2O_3$ catalyst catalyst under default conditions (493 K, 50 bar and 0.17 kg catalyst).

| Species (mol.s$^{-1}$) | Bed 1 | Bed 2 | Bed 3 | Bed 4 | Bed 5 |
|---|---|---|---|---|---|
| $F_{CO}$ ($\times 10$) | 1.32 | 1.25 | 1.20 | 1.15 | 1.12 |
| $F_{H_2}$ ($\times 10$) | 3.33 | 3.17 | 3.05 | 2.95 | 2.88 |
| $F_{CO_2}$ ($\times 10^2$) | 3.21 | 3.13 | 3.09 | 3.07 | 3.07 |
| $F_{H_2O}$ ($\times 10^3$) | 1.92 | 3.06 | 3.79 | 4.25 | 4.52 |
| $F_{CH_3OH}$ ($\times 10^2$) | 1.22 | 1.92 | 2.45 | 2.86 | 3.20 |
| $F_{DME}$ ($\times 10^3$) | 1.78 | 2.09 | 2.37 | 2.64 | 2.89 |
| $F_{CH_4}$ ($\times 10^2$) | 3.61 | 3.61 | 3.61 | 3.61 | 3.61 |
| $F_{N_2}$ ($\times 10$) | 2.51 | 2.51 | 2.51 | 2.51 | 2.51 |
| Total flow-rate ($\times 10$) | 8.01 | 7.86 | 7.74 | 7.65 | 7.57 |

When the one-bed configuration for CZA+$\gamma$-$Al_2O_3$ and CZA+HZSM-5 catalysts are discussed Sections 4.1.1, 4.1.2 and 4.1.3, it was shown that CZA+$\gamma$-$Al_2O_3$ provides slightly higher syngas conversion. However, in multi-bed configurations, as bed number increases, CZA+HZSM-5 compensates the gap between each desired parameter and outweighs CZA+$\gamma$-$Al_2O_3$ at bed-2. The main reason for the change in this pattern is related to the change in the exit flow-rates below. At the beginning of the cascade reactor configuration, HZSM-5 catalyst consumes more methanol produced from the $MS_1$ and $MS_2$ reactions (Reactions 2.1 & 2.2) than HZSM-5 catalyst which, in turn, results in more DME formation and hence more DME yield as well. In addition, since $\gamma$-$Al_2O_3$ has a more tendency of adsorbing water formed as a by-product, the catalyst performance for the DME formation will decrease more than HZSM-5 catalyst [15,34]. Furthermore, HZSM-5 catalyst consists of strong Lewis acid sites, which enables more methanol formation at lower temperatures compared to $\gamma$-$Al_2O_3$ [2,10,34]. These facts explain why DME yield in CZA+HZSM-5 catalyst is significantly higher than that in the CZA+$\gamma$-$Al_2O_3$ case. The change in CO conversion, $CO_2$ conversion and DME yield are both tabulated and illustrated in Tables 4.25 and 4.26.

Table 4.24. Outlet flow-rates (mol/s) for cascade packed-bed reactors for CZA-HZSM-5 catalyst under default conditions (493 K, 50 bar and 0.17 kg catalyst).

| Species | Bed 1 | Bed 2 | Bed 3 |
|---|---|---|---|
| $F_{CO}$ (mol/s)($\times 10$) | 1.32 | 1.24 | 1.18 |
| $F_{H_2}$ (mol/s)($\times 10$) | 3.33 | 3.15 | 3.02 |
| $F_{CO_2}$ (mol/s)($\times 10^2$) | 3.21 | 3.14 | 3.14 |
| $F_{H_2O}$ (mol/s)($\times 10^3$) | 2.12 | 4.88 | 7.67 |
| $F_{CH_3OH}$ (mol/s)($\times 10^2$) | 1.19 | 1.66 | 1.74 |
| $F_{DME}$ (mol/s)($\times 10^3$) | 1.98 | 4.03 | 6.80 |
| $F_{CH_4}$ (mol/s)($\times 10^2$) | 3.61 | 3.61 | 3.61 |
| $F_{N_2}$ (mol/s)($\times 10$) | 2.51 | 2.51 | 2.51 |
| Total flow-rate (mol/s)($\times 10$) | 8.01 | 7.83 | 7.70 |

Table 4.25. CO conversion, $CO_2$ conversion and DME yield (%) with respect to bed number for CZA+$\gamma$-$Al_2O_3$ catalyst.

| Bed | CO conversion (%) | $CO_2$ conversion (%) | DME yield (%) |
|---|---|---|---|
| 1 | 6.3 | 4.3 | 2.04 |
| 2 | 11.1 | 6.8 | 2.39 |
| 3 | 14.9 | 8.2 | 2.71 |
| 4 | 18.1 | 8.7 | 3.02 |
| 5 | 20.8 | 8.8 | 3.31 |

Table 4.26. CO conversion, $CO_2$ conversion and DME yield (%) with respect to bed number for CZA+HZSM-5 catalyst.

| Bed | CO conversion (%) | $CO_2$ conversion (%) | DME yield (%) |
|---|---|---|---|
| 1 | 6.1 | 4.2 | 1.79 |
| 2 | 12.1 | 6.4 | 4.61 |
| 3 | 16.6 | 6.5 | 7.80 |

The temperature profile of the cascade reactor systems for CZA+$\gamma$-$Al_2O_3$ and CZA+HZSM-5 cases can be seen from Figures 4.1 and 4.2. As the bed number increase, the bed temperature profile's slope becomes less steep. Also, the exit temperature of each bed decreases with an increase in the bed number. These facts can be associated with the consumption of the carbon gases and water formation due to $MS_2$ MD reactions. With water formation, the shift to RWGS reaction, which is a moderate endothermic response, is likely to occur due to thermodynamic constraint. As a result, temperature rise becomes slower, and the maximum temperature at the outlet is lower.

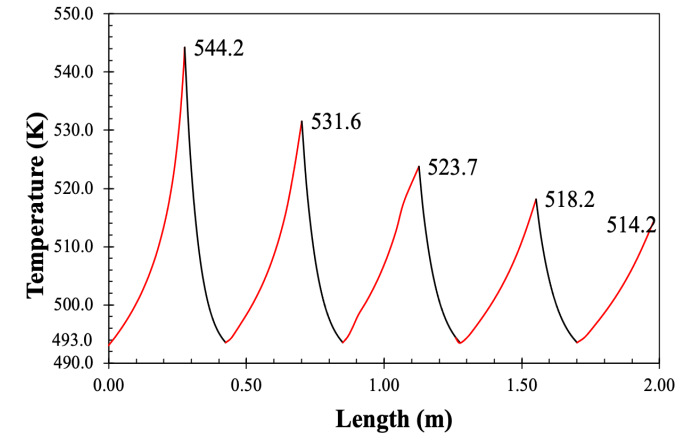


Figure 4.1. Temperature profile of cascade reactor system for CZA+$\gamma$-$Al_2O_3$.

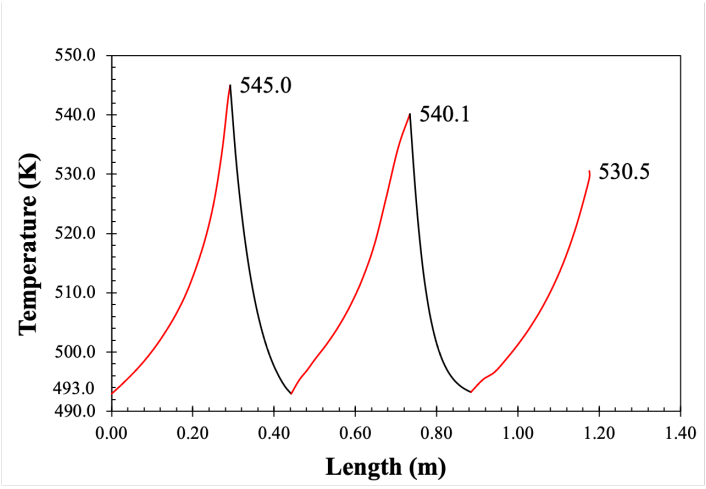


Figure 4.2. Temperature profile of cascade reactor system for CZA+HZSM-5

The microchannel heat-exchangers' length is determined as 0.15 m under default conditions for both catalysts, and the overall length of the cascade reactor system for CZA+$\gamma$-$Al_2O_3$ and CZA+HZSM-5 is estimated as 1.98 and 1.18 m, respectively.

## 4.4. Biomass Composition Effect on Adiabatic Packed-Bed Reactors in Cascade Reactor System

Globally, the source of syngas release is mainly comprised of biomass-based and reforming facilities [34, 68]. In literature, most of the studies focus only on the reforming based syngas release; hence they do evaluate the waste as the upstream of their processes. In this section, impacts of the differences in the composition of biomass and reforming syngas on CO and $CO_2$ conversions, and DME yield are studied. In Table 4.27, which compares two different scenarios of inlet compositions, the most noticeable difference is observed in the composition of $H_2$. The reforming based facility releases a syngas comprises approximately 40% whereas this ratio is only around 17% for the biomass-based facility. Another striking composition change is seen in $N_2$ which is fed as inert for both cases. The biomass-based syngas includes almost 50% of $N_2$ whereas reforming-based syngas comprises only a third of the overall feed. The CO compositions are close to one another, 0.1716 and 0.208 for the reforming and biomass syngas respectively [15, 68]. Composition of $CO_2$ is stated as 0.0409 and 0.103 for reforming and biomass-based syngases respectively [15, 68].

When the results from both compositions are discussed in detail, the biomass-based simulations perform much inefficient than the default composition due to the significantly lower hydrogen content (Table 4.28). Since both methanol formation reactions (2.1 and 2.2) are stimulated with the presence of hydrogen, the lack of hydrogen requires a considerable amount of catalyst loaded in the packed-bed. However, it should be noted that the overall pressure drop is taken into account and specified to 10%. So, the inlet temperature for biomass-based compositions is increased in order to obtain a proper simulation based on the pressure drop criteria.

Table 4.27. Molar compositions of each species for default and biomass case [15, 68].

| Species | Default composition | Biomass composition |
|---|---|---|
| CO | 0.1716 | 0.208 |
| $H_2$ | 0.4325 | 0.174 |
| $CO_2$ | 0.0409 | 0.103 |
| $H_2O$ | 0.0002 | 0.0002 |
| $CH_3OH$ | 0.003 | 0.003 |
| DME | 0.0018 | 0.0018 |
| $CH_4$ | 0.0440 | 0.017 |
| $N_2$ | 0.3060 | 0.493 |

Table 4.28. Bed configuration for biomass composition for CZA+HZSM-5 catalyst.

| Case number | Maximum bed number | $L_{react}$ (m) | $w_{cat}$ (kg) | Pressure drop (bar) | $T_{in}$ (K) | $T_{out}$ (K) |
|---|---|---|---|---|---|---|
| 1 | 1 | 0.75 | 0.44 | 6 | 523.2 | 543.5 |
| 2 | 2 | 0.38 | 0.22 | 2.1 | 533.2 | 543.6 |

Due to pressure drop limitation, the maximum attainable bed number remains considerably lower than the reforming-based syngas composition (Table 4.29). For case 2, the configuration is repeated only for two consecutive packed-bed reactors. The syngas conversion in the default case is approximately ten times higher than of the biomass-based case 2. The DME yield for case 2 is determined as 1.69 % which is approximately 1/8 of the DME yield for the default case, 8.1%.

The effect of water removal ratio biomass-based syngas simulation is also investigated, and the results are tabulated in Table 4.32. As mentioned in Section 4.2, water removal ratio has a very slight influence on both CO conversion and DME yield. The calculations are performed for Case 2 stated in Table 4.28 only because of the pressure drop criteria. Since the biomass composition does not provide higher maximum attainable bed numbers, the effect of water removal ratio on $CO_2$ conversion is insignificant

for biomass composition. Compared to the default case, biomass composition results in extremely lower $CO_2$ conversion, 5.70 and 0.37% respectively.

Table 4.29. CO conversion, $CO_2$ conversion and DME yield of biomass composition for CZA+HZSM-5 catalyst.

| Case number | Maximum bed number | $w_{cat}$ (kg) | $T_{out}$ (K) | CO conversion (%) | $CO_2$ conversion (%) | DME yield (%) |
|---|---|---|---|---|---|---|
| 1 | 1 | 0.75 | 543.5 | 1.71 | 0.33 | 1.67 |
| 2 | 2 | 0.44 | 543.6 | 1.75 | 0.35 | 1.69 |

Table 4.30. Effect of water removal percentage on CO conversion (%) for CZA+HZSM-5 catalyst in biomass composition.

| Number of bed | 30 % water removal | Stage-wise % water removal | First 2 30 % then last 3 50 % | First 3 50 % then last 2 30 % |
|---|---|---|---|---|
| 1 | 0.90 | 0.90 | 0.90 | 0.90 |
| 2 | 1.75 | 1.75 | 1.75 | 1.75 |

Table 4.31. Effect of water removal percentage on $CO_2$ conversion (%) for CZA+HZSM-5 catalyst in biomass composition.

| Number of bed | 30 % water removal | Stage-wise % water removal | First 2 30 % then last 3 50 % | First 3 50 % then last 2 30 % |
|---|---|---|---|---|
| 1 | 0.19 | 0.19 | 0.19 | 0.19 |
| 2 | 0.35 | 0.36 | 0.36 | 0.37 |

This section suggests that the lack in hydrogen composition affects the cascade reactor system configuration negatively in terms of the syngas composition and DME yield. If the hydrogen amount can be increased in the biomass-composition such as a membrane heat-exchanger with hydrogen permeability and water removal, the system

may result in much higher syngas conversion and DME yield. Alternatively, the inlet biomass-based feed can be supported with pure hydrogen stream to enhance the carbon oxide conversions and DME yield.

Table 4.32. Effect of water removal percentage on DME yield for CZA+HZSM-5 catalyst in biomass composition.

| Number of bed | 30 % water removal | Stage-wise % water removal | First 2 30 % then last 3 50 % | First 3 50 % then last 2 30 % |
|---|---|---|---|---|
| 1 | 1.33 | 1.33 | 1.33 | 1.33 |
| 2 | 1.69 | 1.69 | 1.69 | 1.70 |

### 4.5. Microchannel Heat-Exchangers in Cascade Reactor System

The 2D countercurrent microchannel heat-exchangers are designed and simulated in order to satisfy the required cooling of the reactor outlet in the ANSYS platform. Gambit software (version 2.3.16) is used for the composition of geometry and meshing, and ANSYS 19.2 is used for the numerical solution of the set of partial differential equations (PDEs) of the heat exchanger model via the finite volume method. Computations are carried out on an HP Z800 workstation equipped with 48 GB of memory. The number of cells constructed in the fluid and sweep zones is equal to 276000 (per zones). The reported temperature values are calculated by taking the average surface area integral of the channel cross-section normal to fluid flow.

The composition of the channel fluids is determined from the exit of the preceding packed-bed reactor. The detailed modeling of microchannel heat-exchangers is described in Section 3.1.2 in elaborate. The microchannel heat-exchangers are designed for both CZA+$\gamma$-$Al_2O_3$ and CZA+HZSM-5 catalyst configurations with the consideration of pressure drop. As mentioned in Section 4.3, for CZA+$\gamma$-$Al_2O_3$ and CZA+HZSM-5 catalyst configurations, the number of packed-bed is limited with 5 and 3, respectively. For that reason, only four and two microchannel heat-exchangers are

required for the temperature regulation of the adiabatic cascade reactor bed configuration, respectively. It should be noted that the pressure drop is negligible (i.e. $< 1$ %) along the channel length.

The microchannels' height and width are chosen as $3\times10^{-4}$ m and $6\times10^{-4}$ m. A detailed explanation for the basis of selection of height and width is provided in Section 3.1.2. The channel length for the default configuration is determined as $15\times10^{-2}$ m for the desired cooling. With this configuration, 41218 microchannel (20609 fluid, 20609 sweep channel) is sufficient for cooling the packed-beds' outlet stream. By trial and error, the sweep and reactor outlet fluid velocity is set to 0.25 and 0.2 m/s, respectively.

The default design parameters for the microchannel heat-exchanger are determined as follows: Stainless steel as wall material, 0.002 m as wall thickness, syngas with the same composition of the reactor inlet as the sweep gas type. Here, "wall" refers to the solid zone separating the channels and "material" refers to the material of construction of the heat-exchanger block. The simulations showed that the wall thickness within the heating and cooling channels has a negligible effect on the heat transfer rate. Therefore, the default case with 0.002 m thickness is chosen for the optimum design.

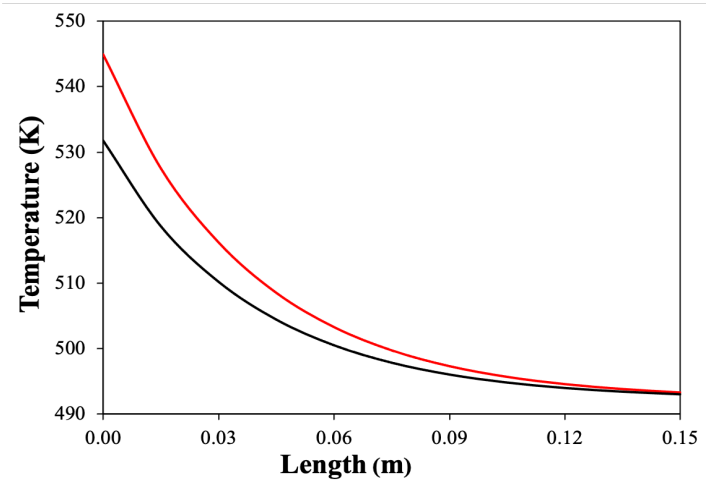


Figure 4.3. Temperature profile of the first microchannel-hex for reaction outlet (red) and sweep gas (black).

Similar to the wall thickness effect, wall material plays an insignificant role in the temperature profile shown in Figure 4.3. This finding is obtained by simulating the heat- exchanger with different materials presented in Table 3.5. This fact is explained due to sufficient channel length and contact of sweep and reactor outlet flow-rate. The wall material is chosen as stainless steel due to its durability, resistance to water corrosion, ease of fabrication, and total life-cycle costs [31].

Finally, the syngas composition fed to the packed-bed is used as a default sweep gas in the microchannel heat-exchangers rather than pure hydrogen or air. Due to the same reasons stated in the previous paragraphs, the reaction outlet channel's exit temperature converges around 493 K illustrated in Figure 4.3. The use of pure hydrogen is disadvantageous economically. Since syngas is fed to the microchannel at 493 K, which is the same as the first packed-bed's inlet temperature, no additional heating or cooling cost is needed. On the other hand, extra preheating for air to 493 K is required for an optimum microchannel heat-exchanger performance.

# 5. CONCLUSION

## 5.1. Conclusions

In the scope of this research, the process of DME synthesis from syngas is conducted via the modelling of adiabatic packed-bed reactors integrated with the microchannel heat-exchangers. The design of the 1D pseudo-homogeneous packed-bed reactor model is constructed for the direct DME synthesis performed with bifunctional catalysis in the MATLAB platform. The packed-bed reactor dimensions are determined as 0.17 kg catalyst per bed, 0.28 m and 0.29 m in terms of length and 0.025 m in terms of diameter for 1:1 (by mass) physical mixtures of CZA+$\gamma$-$Al_2O_3$ and CZA+HZSM-5 bifunctional catalysts respectively.

The simulations of 2D countercurrent intercooling microchannel heat-exchanger design, on the other hand, are performed via ANSYS, which estimates the outputs based on both conservation of mass and momentum principles under the finite-volume method. The channel width and wall thickness are set to $6\times10^{-4}$ and $2\times10^{-3}$ m respectively. Both sweep and reactor downstream channels' height are chosen as $3\times10^{-4}$ m. By optimizing the superficial velocity of both sweep and reactor fluid channels in the microchannel countercurrently, the channel length is determined as $1.5\times10^{-1}$ m at which the temperature of the hot fluid reaches to 493.15 K, the inlet condition for the second packed-bed reactor. The major findings of this research based on the packed-bed reactor and microchannel heat-exchanger can be summarized in the following conclusions:

- The results demonstrate a significant effect of bifunctionality of the catalyst on the packed-bed configuration for both methanol dehydration catalysts. The syngas conversion (both CO and $CO_2$) increases in the mixed bed configuration more than 4 times that of 2 consecutive bed configuration for CZA+$\gamma$-$Al_2O_3$ case. The DME yield improve from 1.8 to 2.1% for CZA+$\gamma$-$Al_2O_3$ and 2.0 to 2.3% for CZA-HZSM-5 bifunctional catalysts respectively.

- Compared with $Cu/ZnO-Al_2O_3$, as the CZA- HZSM-5 catalyst provides higher methanol activity due to its stronger acidic sites, more desirable results are obtained in the syngas conversion and the DME yield. Under the same inlet conditions, at 493 K and 50 bar, the overall conversion of CO, $CO_2$ and DME yield are 17.2, 6.7 and 8.1% at the end of bed 3 for CZA- HZSM-5 and 21.6, 9.2 and 2.1% at the end of bed 5 for $Cu/ZnO-Al_2O_3$. The present results confirm the fact that CZA- HZSM-5 produces a better performance than $Cu/ZnO-Al_2O_3$ in terms of the syngas conversion and DME yield.
- Elevation in the operating temperature leads to a positive impact on the syngas conversion. However, DME yield tends to decrease at the temperature higher than 488 K. Also, in order to obtain a significant ratio of syngas conversion, the less inlet temperature refers to the more weight of catalyst loaded to the bed, which makes the DME synthesis process less feasible. With the range of 473-488 K inlet temperature 0.63-0.32 kg catalyst should be loaded to the bed, which almost doubles the default catalyst weight value (0.17 kg). In this respect, the optimal inlet temperature range is determined as 488 to 498 K based on the studies conducted for both $Cu/ZnO-Al_2O_3$ and CZA- HZSM-5 bifunctional catalysts.
- The results on the pressure effect are broadly consistent with both the literature and thermodynamics. An increase in pressure significantly affects the syngas conversion and DME yield for both $Cu/ZnO-Al_2O_3$ and CZA- HZSM-5 bifunctional catalysts. For HZSM-5, at 20 bar, with the bed number of 4 and 0.17 kg catalyst loaded in each bed, the overall conversion of CO, $CO_2$ and DME yield are obtained as 8.1, 3.5 and 3.0% . On the other hand, at 60 bar, much higher syngas conversion and DME yield values are obtained with only 3 consecutive packed-beds (18.5, 7.8 and 9.0 %).
- The CO conversion and DME yield are proportional to the amount of catalyst loaded in the packed-bed. Due to CO hydrogenation, $CO_2$conversion hampers after a 0.17 kg of catalyst loaded in each bed. Also, the more weight of the catalyst, the more temperature rise in the reactor due to exothermic reactions. Hence, 0.17 kg is the maximum amount at which both catalyst deactivation and

methane formation are omitted.

## 5.2. Recommendations

- The 1D pseudo homogeneous model can be converted to the 1D heterogeneous model by including the interactions with the catalyst particles and the bulk fluid.
- The dimensions of both the 1D packed-bed reactor and 2D microchannel heat-exchanger design can be enhanced to 2D and 3D respectively.
- In the design of microchannel heat-exchanger, a selective SOD membrane can be inserted to verify the results obtained in this study hypothetically.

# REFERENCES


1. Ritchie, H. and M. Roser, *$CO_2$ and Greenhouse Gas Emissions*, 2017, https://ourworldindata.org/co2-and-other-greenhouse-gas-emissions, September 2020.

2. Catizzone, E., G. Bonura, M. Migliori, F. Frusteri and G. Giordano, "$CO_2$ recycling to dimethyl ether: State-of-the-art and perspectives", *Molecules*, Vol. 23, No. 1, p. 31, 2018.

3. Zhou, P. and M. Wang, "Carbon dioxide emissions allocation: A review", *Ecological Economics*, Vol. 125, pp. 47–59, 2016.

4. de Coninck, H. and S. M. Benson, "Carbon dioxide capture and storage: issues and prospects", *Annual Review of Environment and Resources*, Vol. 39, pp. 243–270, 2014.

5. Agency, U. S. E. P., *Greenhouse Gas Emissions*, 2017, https://www.epa.gov/ghgemissions/sources-greenhouse-gas-emissions, July 2020.

6. Yoro, K. O. and M. O. Daramola, "$CO_2$ emission sources, greenhouse gases, and the global warming effect", *Advances in Carbon Capture*, pp. 3–28, Elsevier, 2020.

7. Tseng, S.-C. and S.-W. Hung, "A strategic decision-making model considering the social costs of carbon dioxide emissions for sustainable supply chain management.", *Journal of Environmental Management*, Vol. 133, pp. 315–322, 2014.

8. of Energy Efficiency & Renewable Energy, O., *Biofuel Basics*, https://www.energy.gov/eere/bioenergy/biofuels-basics, July 2020.

9. Shell, *Biofuels*, https://www.shell.com/energy-and-innovation/new-energies/

biofuels.html, July 2020.

10. Rahimpour, M. R., M. Farniaei, M. Abbasi, J. Javanmardi and S. Kabiri, "Comparative study on simultaneous production of methanol, hydrogen, and DME using a novel integrated thermally double-coupled reactor", *Energy & Fuels*, Vol. 27, No. 4, pp. 1982–1993, 2013.

11. Lee, S. B., W. Cho, D. K. Park and E. S. Yoon, "Simulation of fixed bed reactor for dimethyl ether synthesis", *Korean Journal of Chemical Engineering*, Vol. 23, No. 4, pp. 522–530, 2006.

12. Azizi, Z., M. Rezaeimanesh, T. Tohidian and M. R. Rahimpour, "Dimethyl ether: A review of technologies and production challenges", *Chemical Engineering and Processing: Process Intensification*, Vol. 82, pp. 150–172, 2014.

13. Organization, W. H., *Greenhouse Gas Emissions*, 2017, http://www.inchem.org/documents/icsc/icsc/eics1561.htm, July 2020.

14. Venvik, H. J. and J. Yang, "Catalysis in microstructured reactors: Short review on small-scale syngas production and further conversion into methanol, DME and Fischer-Tropsch products", *Catalysis Today*, Vol. 285, pp. 135–146, 2017.

15. Vakili, R., E. Pourazadi, P. Setoodeh, R. Eslamloueyan and M. Rahimpour, "Direct dimethyl ether (DME) synthesis through a thermally coupled heat exchanger reactor", *Applied Energy*, Vol. 88, No. 4, pp. 1211–1223, 2011.

16. An, X., Y.-Z. Zuo, Q. Zhang, D.-z. Wang and J.-F. Wang, "Dimethyl ether synthesis from $CO_2$ hydrogenation on a CuO- ZnO- $Al_2O_3$- $ZrO_2$/HZSM-5 bifunctional catalyst", *Industrial & Engineering Chemistry Research*, Vol. 47, No. 17, pp. 6547–6554, 2008.

17. Chen, W.-H., C.-L. Hsu and X.-D. Wang, "Thermodynamic approach and comparison of two-step and single step DME (dimethyl ether) syntheses with carbon

dioxide utilization", *Energy*, Vol. 109, pp. 326–340, 2016.

18. Peláez, R., P. Marín and S. Ordóñez, "Direct synthesis of dimethyl ether from syngas over mechanical mixtures of $CuO/ZnO/Al_2O_3$ and $\gamma$-$Al_2O_3$: Process optimization and kinetic modelling", *Fuel Processing Technology*, Vol. 168, pp. 40–49, 2017.

19. Aguayo, A. T., J. Erena, D. Mier, J. M. Arandes, M. Olazar and J. Bilbao, "Kinetic modeling of dimethyl ether synthesis in a single step on a CuO- ZnO- $Al_2O_3$/$\gamma$-$Al_2O_3$ catalyst", *Industrial & Engineering Chemistry Research*, Vol. 46, No. 17, pp. 5522–5530, 2007.

20. Ozturk, N. F. and A. K. Avci, "Intensified dimethyl ether production from synthesis gas with $CO_2$", *Chemical Engineering Journal*, Vol. 370, pp. 885–896, 2019.

21. Judy, J., D. Maynes and B. Webb, "Characterization of frictional pressure drop for liquid flows through microchannels", *International Journal of Heat and Mass Transfer*, Vol. 45, No. 17, pp. 3477–3489, 2002.

22. Fan, Y. and L. Luo, "Recent applications of advances in microchannel heat exchangers and multi-scale design optimization", *Heat Transfer Engineering*, Vol. 29, No. 5, pp. 461–474, 2008.

23. Herwig, H., "Momentum and heat transfer in microsized devices", *Micro Process Engineering: Fundamentals, Devices, Fabrication, and Applications*, pp. 47–70, 2006.

24. Karakaya, M. and A. K. Avci, "Comparison of compact reformer configurations for on-board fuel processing", *International Journal of Hydrogen Energy*, Vol. 35, No. 6, pp. 2305–2316, 2010.

25. Onsan, Z. I. and A. K.Avci, *Reactor design for fuel processing." Fuel Cells: Technologies for Fuel Processing.*, Elsevier, 2011.

26. Avcı, A. K., D. L. Trimm and M. Karakaya, "Microreactor catalytic combustion for chemicals processing", *Catalysis Today*, Vol. 155, No. 1-2, pp. 66–74, 2010.

27. of Michigan, U., *Packed Bed Reactors*, `https://encyclopedia.che.engin.umich.edu/Pages/Reactors/PBR/PBR.html`, November 2020.

28. Comsol, *Packed-bed reactor*, `https://www.comsol.com/blogs/packed-bed-reactor/`, November 2020.

29. Fogler, H. S., *Essentials of Chemical Reaction Engineering*, Pearson Education, 2010.

30. Fazlollahnejad, M., M. Taghizadeh, A. Eliassi and G. Bakeri, "Experimental study and modeling of an adiabatic fixed-bed reactor for methanol dehydration to dimethyl ether", *Chinese Journal of Chemical Engineering*, Vol. 17, No. 4, pp. 630–634, 2009.

31. Sinnott, R. and G. Towler, *Chemical Engineering Design: SI Edition*, Butterworth-Heinemann, 2019.

32. Tavan, Y., S. H. Hosseini, M. Ghavipour, M. R. K. Nikou and A. Shariati, "From laboratory experiments to simulation studies of methanol dehydration to produce dimethyl ether—Part I: Reaction kinetic study", *Chemical Engineering and Processing: Process Intensification*, Vol. 73, pp. 144–150, 2013.

33. Tavan, Y. and S. H. Hosseini, "From laboratory experiments to simulation studies of methanol dehydration to produce dimethyl ether reaction—Part II: Simulation and cost estimation", *Chemical Engineering and Processing: Process Intensification*, Vol. 73, pp. 151–157, 2013.

34. Mondal, U. and G. D. Yadav, "Perspective of dimethyl ether as fuel: Part I. Catalysis", *Journal of $CO_2$ Utilization*, Vol. 32, pp. 299–320, 2019.

35. Ohadi, M., K. Choo, S. Dessiatoun and E. Cetegen, *Next Generation Microchannel Heat Exchangers*, Springer, 2013.

36. Foli, K., T. Okabe, M. Olhofer, Y. Jin and B. Sendhoff, "Optimization of micro heat exchanger: CFD, analytical approach and multi-objective evolutionary algorithms", *International Journal of Heat and Mass Transfer*, Vol. 49, No. 5-6, pp. 1090–1099, 2006.

37. Hayer, F., H. Bakhtiary-Davijany, R. Myrstad, A. Holmen, P. Pfeifer and H. J. Venvik, "Synthesis of dimethyl ether from syngas in a microchannel reactor—simulation and experimental study", *Chemical Engineering Journal*, Vol. 167, No. 2-3, pp. 610–615, 2011.

38. Saha, S. K. and G. P. Celata, *Critical Heat Flux in Flow Boiling in Microchannels*, Springer, 2015.

39. Hrnjak, P. and X. Tu, "Single phase pressure drop in microchannels", *International Journal of Heat and Fluid Flow*, Vol. 28, No. 1, pp. 2–14, 2007.

40. Su, H., H. Niu, L. Pan, S. Wang, A. Wang and Y. Hu, "The characteristics of pressure drop in microchannels", *Industrial & Engineering Chemistry Research*, Vol. 49, No. 8, pp. 3830–3839, 2010.

41. Kockmann, N., "Transport processes and exchange equipment", *Micro Process Engineering: Fundamentals, Devices, Fabrication, and Applications*, pp. 71–113, 2006.

42. Álvarez, A., A. Bansode, A. Urakawa, A. V. Bavykina, T. A. Wezendonk, M. Makkee, J. Gascon and F. Kapteijn, "Challenges in the greener production of formates/formic acid, methanol, and DME by heterogeneously catalyzed $CO_2$ hydrogenation processes", *Chemical Reviews*, Vol. 117, No. 14, pp. 9804–9838, 2017.

43. TOYO, *DME (Dimethly Ether)*, `www.toyo-eng.com/jp/en/products/energy`

/dme/, February 2021.

44. Pontzen, F., W. Liebner, V. Gronemann, M. Rothaemel and B. Ahlers, "$CO_2$-based methanol and DME–Efficient technologies for industrial scale production", *Catalysis Today*, Vol. 171, No. 1, pp. 242–250, 2011.

45. Zhu, Y., S. Wang, X. Ge, Q. Liu, Z. Luo and K. Cen, "Experimental study of improved two step synthesis for DME production", *Fuel Processing Technology*, Vol. 91, No. 4, pp. 424–429, 2010.

46. Saravanan, K., H. Ham, N. Tsubaki and J. W. Bae, "Recent progress for direct synthesis of dimethyl ether from syngas on the heterogeneous bifunctional hybrid catalysts", *Applied Catalysis B: Environmental*, Vol. 217, pp. 494–522, 2017.

47. Nakamura, J., I. Nakamura, T. Uchijima, Y. Kanai, T. Watanabe, M. Saito and T. Fujitani, "Methanol synthesis over a Zn-deposited copper model catalyst", *Catalysis Letters*, Vol. 31, No. 4, pp. 325–331, 1995.

48. da Silva, R. J., A. F. Pimentel, R. S. Monteiro and C. J. Mota, "Synthesis of methanol and dimethyl ether from the $CO_2$ hydrogenation over Cu· ZnO supported on $Al_2O_3$ and $Nb_2O_5$", *Journal of $CO_2$ Utilization*, Vol. 15, pp. 83–88, 2016.

49. Mondal, U. and G. D. Yadav, "Perspective of dimethyl ether as fuel: Part II-analysis of reactor systems and industrial processes", *Journal of $CO_2$ Utilization*, Vol. 32, pp. 321–338, 2019.

50. Sousa-Aguiar, E. F., L. G. Appel and C. Mota, "Natural gas chemical transformations: The path to refining in the future", *Catalysis Today*, Vol. 101, No. 1, pp. 3–7, 2005.

51. Bhattacharya, S., K. B. Kabir and K. Hein, "Dimethyl ether synthesis from Victorian brown coal through gasification–Current status, and research and development needs", *Progress in Energy and Combustion Science*, Vol. 39, No. 6, pp. 577–605,

2013.

52. Naik, S. P., T. Ryu, V. Bui, J. D. Miller, N. B. Drinnan and W. Zmierczak, "Synthesis of DME from $CO_2/H_2$ gas mixture", *Chemical Engineering Journal*, Vol. 167, No. 1, pp. 362–368, 2011.

53. Tao, J.-L., K.-W. Jun and K.-W. Lee, "Co-production of dimethyl ether and methanol from CO2 hydrogenation: development of a stable hybrid catalyst", *Applied Organometallic Chemistry*, Vol. 15, No. 2, pp. 105–108, 2001.

54. Liu, D., C. Yao, J. Zhang, D. Fang and D. Chen, "Catalytic dehydration of methanol to dimethyl ether over modified $\gamma$-$Al_2O_3$ catalyst", *Fuel*, Vol. 90, No. 5, pp. 1738–1742, 2011.

55. Xu, M., J. H. Lunsford, D. W. Goodman and A. Bhattacharyya, "Synthesis of dimethyl ether (DME) from methanol over solid-acid catalysts", *Applied Catalysis A: General*, Vol. 149, No. 2, pp. 289–301, 1997.

56. Yaripour, F., F. Baghaei, I. Schmidt and J. Perregaard, "Catalytic dehydration of methanol to dimethyl ether (DME) over solid-acid catalysts", *Catalysis Communications*, Vol. 6, No. 2, pp. 147–152, 2005.

57. Jun, K.-W., H.-S. Lee, H.-S. Roh and S.-E. Park, "Highly water-enhanced HZSM-5 catalysts for dehydration of methanol to dimethyl ether", *Bulletin-Korean Chemical Society*, Vol. 24, No. 1, pp. 106–108, 2003.

58. Vishwanathan, V., K.-W. Jun, J.-W. Kim and H.-S. Roh, "Vapour phase dehydration of crude methanol to dimethyl ether over Na-modified HZSM-5 catalysts", *Applied Catalysis A: General*, Vol. 276, No. 1-2, pp. 251–255, 2004.

59. Moradi, G. R., R. Ghanei and F. Yaripour, "Determination of the optimum operating conditions for direct synthesis of dimethyl ether from syngas", *International Journal of Chemical Reactor Engineering*, Vol. 5, No. 1, 2007.

60. De Falco, M., M. Capocelli and A. Basile, "Selective membrane application for the industrial one-step DME production process fed by $CO_2$ rich streams: Modeling and simulation", *International Journal of Hydrogen Energy*, Vol. 42, No. 10, pp. 6771–6786, 2017.

61. De Falco, M., M. Capocelli and G. Centi, "Dimethyl ether production from $CO_2$ rich feedstocks in a one-step process: thermodynamic evaluation and reactor simulation", *Chemical Engineering Journal*, Vol. 294, pp. 400–409, 2016.

62. Hu, Y., Z. Nie and D. Fang, "Simulation and model design of pipe-shell reactor for the direct synthesis of dimethyl ether from syngas", *Journal of Natural Gas Chemistry*, Vol. 17, No. 2, pp. 195–200, 2008.

63. Lu, W.-Z., L.-H. Teng and W.-D. Xiao, "Simulation and experiment study of dimethyl ether synthesis from syngas in a fluidized-bed reactor", *Chemical Engineering Science*, Vol. 59, No. 22-23, pp. 5455–5464, 2004.

64. You, Q., Z. Liu, W. Li and X. Zhou, "Synthesis of dimethyl ether from methane mediated by HBr", *Journal of Natural Gas Chemistry*, Vol. 18, No. 3, pp. 306–311, 2009.

65. Bai, Z., H. Ma, H. Zhang, W. Ying and D. Fang, "Process simulation of dimethyl ether synthesis via methanol vapor phase dehydration", *Polish Journal of Chemical Technology*, Vol. 15, No. 2, pp. 122–127, 2013.

66. Papari, S., M. Kazemeini and M. Fattahi, "Mathematical modeling of a slurry reactor for DME direct synthesis from syngas", *Journal of Natural Gas Chemistry*, Vol. 21, No. 2, pp. 148–157, 2012.

67. Hu, J., Y. Wang, C. Cao, D. C. Elliott, D. J. Stevens and J. F. White, "Conversion of biomass syngas to DME using a microchannel reactor", *Industrial & Engineering Chemistry Research*, Vol. 44, No. 6, pp. 1722–1727, 2005.

68. Wan, C., F. Yu, Y. Zhang, Q. Li and J. Wooten, "Material balance and energy balance analysis for syngas generation by a pilot-plant scale downdraft gasifier", *Journal of Biobased Materials and Bioenergy*, Vol. 7, No. 6, pp. 690–695, 2013.

69. Metcalf, W., "Metcalf and Eddy wastewater engineering: treatment and reuse", *Wastewater Engineering: Treatment and Reuse. McGraw Hill, New York, NY. https://doi. org/10.1016/0309-1708 (80)*, pp. 90067–6, 2003.

70. J M Smith, M. M. A., H C Van Ness, *Introduction to Chemical Engineering Thermodynamics*, ACS Publications, 2005.

71. McBride, B. J., *Coefficients for calculating thermodynamic and transport properties of individual species*, Vol. 4513, NASA Langley Research Center, 1993.

72. Poling, B. E., J. M. Prausnitz, J. P. O'connell *et al.*, *The Properties of Gases and Liquids*, Vol. 5, Mcgraw-hill New York, 2001.

73. of Chemical, E. A. I., *Thermodynamic Properties of Multicomponent Systems, Multicomponent Phase Equilibria and Chemical Equilibria*, American Institute of Chemical Engineers, 1982.

74. Bac, S. and A. K. Avci, "Ethylene oxide synthesis in a wall-coated microchannel reactor with integrated cooling", *Chemical Engineering Journal*, Vol. 377, p. 120104, 2019.

75. Kolb, G., "Microstructured reactors for distributed and renewable production of fuels and electrical energy", *Chemical Engineering and Processing: Process Intensification*, Vol. 65, pp. 1–44, 2013.

76. Uriz, I., G. Arzamendi, E. Lopez, J. Llorca and L. Gandía, "Computational fluid dynamics simulation of ethanol steam reforming in catalytic wall microchannels", *Chemical Engineering Journal*, Vol. 167, No. 2-3, pp. 603–609, 2011.

77. Toolbox, E., *Thermal conductivity of common metals, metallic elements and Alloys*, 2017, https://www.engineeringtoolbox.com, September 2020.

78. Shelton, S., "Thermal conductivity of some irons and steels over the temperature range 100 to 500 C", *Bureau of Standards Journal of research*, Vol. 12, No. 4/6, pp. 441–450, 1934.

79. Elements, A., *Cordierite*, https://www.americanelements.com/cordierite, September 2020.

# APPENDIX A: COPYRIGHTS OF FIGURES

ELSEVIER LICENSE
TERMS AND CONDITIONS

Feb 23, 2021

---

This Agreement between Bogazici University -- Ceren Hatipoglu ("You") and Elsevier ("Elsevier") consists of your license details and the terms and conditions provided by Elsevier and Copyright Clearance Center.

| | |
|---|---|
| License Number | 5014940910127 |
| License date | Feb 23, 2021 |
| Licensed Content Publisher | Elsevier |
| Licensed Content Publication | Elsevier Books |
| Licensed Content Title | Advances in Carbon Capture |
| Licensed Content Author | Kelvin O. Yoro,Michael O. Daramola |
| Licensed Content Date | Jan 1, 2020 |
| Licensed Content Pages | 26 |
| Start Page | 3 |
| End Page | 28 |
| Type of Use | reuse in a thesis/dissertation |



Figure A.1. Copyrights of Figure 1.1 (page 1)

| | |
|---|---|
| Portion | figures/tables/illustrations |
| Number of figures/tables/illustrations | 1 |
| Format | both print and electronic |
| Are you the author of this Elsevier chapter? | No |
| Will you be translating? | No |
| Title | MULTIPLE ADIABATIC BEDS FOR EFFICIENT CONVERSION OF CO2-CONTAINING SYNGAS TO DIMETHYL ETHER |
| Institution name | Bogazici University |
| Expected presentation date | Feb 2021 |
| Portions | Figure 1.5 |
| Requestor Location | Bogazici University<br>Bogazici University<br>Department of Chemical Engineering<br><br>Istanbul, 34342<br>Turkey<br>Attn: Bogazici University |
| Publisher Tax ID | GB 494 6272 12 |
| Total | 0.00 USD |
| Terms and Conditions | |

Figure A.2. Copyrights of Figure 1.1 (page 2).

ELSEVIER LICENSE
TERMS AND CONDITIONS

Feb 23, 2021

This Agreement between Bogazici University -- Ceren Hatipoglu ("You") and Elsevier ("Elsevier") consists of your license details and the terms and conditions provided by Elsevier and Copyright Clearance Center.

| | |
|---|---|
| License Number | 5014860925795 |
| License date | Feb 23, 2021 |
| Licensed Content Publisher | Elsevier |
| Licensed Content Publication | International Journal of Hydrogen Energy |
| Licensed Content Title | Comparison of compact reformer configurations for on-board fuel processing |
| Licensed Content Author | Mustafa Karakaya,Ahmet K. Avci |
| Licensed Content Date | Mar 1, 2010 |
| Licensed Content Volume | 35 |
| Licensed Content Issue | 6 |
| Licensed Content Pages | 12 |
| Start Page | 2305 |



Figure A.3. Copyrights of Figure 2.1 (page 1).

| | |
|---|---|
| End Page | 2316 |
| Type of Use | reuse in a thesis/dissertation |
| Portion | figures/tables/illustrations |
| Number of figures/tables/illustrations | 1 |
| Format | both print and electronic |
| Are you the author of this Elsevier article? | No |
| Will you be translating? | No |
| Title | MULTIPLE ADIABATIC BEDS FOR EFFICIENT CONVERSION OF CO2-CONTAINING SYNGAS TO DIMETHYL ETHER |
| Institution name | Bogazici University |
| Expected presentation date | Feb 2021 |
| Portions | Figure 2 |
| Requestor Location | Bogazici University<br>Bogazici University<br>Department of Chemical Engineering<br><br>Istanbul, 34342<br>Turkey<br>Attn: Bogazici University |
| Publisher Tax ID | GB 494 6272 12 |



Figure A.4. Copyrights of Figure 2.1 (page 2).

ELSEVIER LICENSE
TERMS AND CONDITIONS

Feb 23, 2021

---

This Agreement between Bogazici University -- Ceren Hatipoglu ("You") and Elsevier ("Elsevier") consists of your license details and the terms and conditions provided by Elsevier and Copyright Clearance Center.

| | |
|---|---|
| License Number | 5014860525573 |
| License date | Feb 23, 2021 |
| Licensed Content Publisher | Elsevier |
| Licensed Content Publication | International Journal of Heat and Mass Transfer |
| Licensed Content Title | Optimization of micro heat exchanger: CFD, analytical approach and multi-objective evolutionary algorithms |
| Licensed Content Author | Kwasi Foli,Tatsuya Okabe,Markus Olhofer,Yaochu Jin,Bernhard Sendhoff |
| Licensed Content Date | Mar 1, 2006 |
| Licensed Content Volume | 49 |
| Licensed Content Issue | 5-6 |
| Licensed Content Pages | 10 |



Figure A.5. Copyrights of Figure 2.2 (page 1).

| | |
|---|---|
| Start Page | 1090 |
| End Page | 1099 |
| Type of Use | reuse in a thesis/dissertation |
| Portion | figures/tables/illustrations |
| Number of figures/tables/illustrations | 1 |
| Format | both print and electronic |
| Are you the author of this Elsevier article? | No |
| Will you be translating? | No |
| Title | MULTIPLE ADIABATIC BEDS FOR EFFICIENT CONVERSION OF CO2-CONTAINING SYNGAS TO DIMETHYL ETHER |
| Institution name | Bogazici University |
| Expected presentation date | Feb 2021 |
| Portions | Figure 1 |
| Requestor Location | Bogazici University<br>Bogazici University<br>Department of Chemical Engineering<br><br>Istanbul, 34342<br>Turkey<br>Attn: Bogazici University |
| Publisher Tax ID | GB 494 6272 12 |



Figure A.6. Copyrights of Figure 2.2 (page 2).

ELSEVIER LICENSE
TERMS AND CONDITIONS

Feb 23, 2021

---

This Agreement between Bogazici University -- Ceren Hatipoglu ("You") and Elsevier ("Elsevier") consists of your license details and the terms and conditions provided by Elsevier and Copyright Clearance Center.

| | |
|---|---|
| License Number | 5014860107438 |
| License date | Feb 23, 2021 |
| Licensed Content Publisher | Elsevier |
| Licensed Content Publication | Catalysis Today |
| Licensed Content Title | CO2-based methanol and DME – Efficient technologies for industrial scale production |
| Licensed Content Author | Florian Pontzen,Waldemar Liebner,Veronika Gronemann,Martin Rothaemel,Bernd Ahlers |
| Licensed Content Date | Aug 10, 2011 |
| Licensed Content Volume | 171 |
| Licensed Content Issue | 1 |
| Licensed Content Pages | 9 |



Figure A.7. Copyrights of Figure 2.3 and 2.4 (page 1).

| | |
|---|---|
| Start Page | 242 |
| End Page | 250 |
| Type of Use | reuse in a thesis/dissertation |
| Portion | figures/tables/illustrations |
| Number of figures/tables/illustrations | 2 |
| Format | both print and electronic |
| Are you the author of this Elsevier article? | No |
| Will you be translating? | No |
| Title | MULTIPLE ADIABATIC BEDS FOR EFFICIENT CONVERSION OF CO2-CONTAINING SYNGAS TO DIMETHYL ETHER |
| Institution name | Bogazici University |
| Expected presentation date | Feb 2021 |
| Portions | Figure 12, Figure 13 |
| Requestor Location | Bogazici University<br>Bogazici University<br>Department of Chemical Engineering<br><br>Istanbul, 34342<br>Turkey<br>Attn: Bogazici University |
| Publisher Tax ID | GB 494 6272 12 |



Figure A.8. Copyrights of Figure 2.3 and 2.4 (page 2).

ELSEVIER LICENSE
TERMS AND CONDITIONS

Feb 23, 2021

This Agreement between Bogazici University -- Ceren Hatipoglu ("You") and Elsevier ("Elsevier") consists of your license details and the terms and conditions provided by Elsevier and Copyright Clearance Center.

| | |
|---|---|
| License Number | 5014851257257 |
| License date | Feb 23, 2021 |
| Licensed Content Publisher | Elsevier |
| Licensed Content Publication | International Journal of Hydrogen Energy |
| Licensed Content Title | Selective membrane application for the industrial one-step DME production process fed by CO2 rich streams: Modeling and simulation |
| Licensed Content Author | Marcello De Falco,Mauro Capocelli,Angelo Basile |
| Licensed Content Date | Mar 9, 2017 |
| Licensed Content Volume | 42 |
| Licensed Content Issue | 10 |
| Licensed Content Pages | 16 |



Figure A.9. Copyrights of Figure 2.5 (page 1).

| | |
|---|---|
| Start Page | 6771 |
| End Page | 6786 |
| Type of Use | reuse in a thesis/dissertation |
| Portion | figures/tables/illustrations |
| Number of figures/tables/illustrations | 1 |
| Format | both print and electronic |
| Are you the author of this Elsevier article? | No |
| Will you be translating? | No |
| Title | MULTIPLE ADIABATIC BEDS FOR EFFICIENT CONVERSION OF CO2-CONTAINING SYNGAS TO DIMETHYL ETHER |
| Institution name | Bogazici University |
| Expected presentation date | Feb 2021 |
| Portions | Fig. 2 |
| Requestor Location | Bogazici University<br>Bogazici University<br>Department of Chemical Engineering<br><br>Istanbul, 34342<br>Turkey<br>Attn: Bogazici University |
| Publisher Tax ID | GB 494 6272 12 |



Figure A.10. Copyrights of Figure 2.5 (page 2).

ELSEVIER LICENSE
TERMS AND CONDITIONS

Feb 23, 2021

This Agreement between Bogazici University -- Ceren Hatipoglu ("You") and Elsevier ("Elsevier") consists of your license details and the terms and conditions provided by Elsevier and Copyright Clearance Center.

| | |
|---|---|
| License Number | 5014850787101 |
| License date | Feb 23, 2021 |
| Licensed Content Publisher | Elsevier |
| Licensed Content Publication | Applied Energy |
| Licensed Content Title | Direct dimethyl ether (DME) synthesis through a thermally coupled heat exchanger reactor |
| Licensed Content Author | R. Vakili,E. Pourazadi,P. Setoodeh,R. Eslamloueyan,M.R. Rahimpour |
| Licensed Content Date | Apr 1, 2011 |
| Licensed Content Volume | 88 |
| Licensed Content Issue | 4 |
| Licensed Content Pages | 13 |



Figure A.11. Copyrights of Figure 2.6 (page 1).

| | |
|---|---|
| Start Page | 1211 |
| End Page | 1223 |
| Type of Use | reuse in a thesis/dissertation |
| Portion | figures/tables/illustrations |
| Number of figures/tables/illustrations | 1 |
| Format | both print and electronic |
| Are you the author of this Elsevier article? | No |
| Will you be translating? | No |
| Title | MULTIPLE ADIABATIC BEDS FOR EFFICIENT CONVERSION OF CO2-CONTAINING SYNGAS TO DIMETHYL ETHER |
| Institution name | Bogazici University |
| Expected presentation date | Feb 2021 |
| Portions | Figure 1 |
| Requestor Location | Bogazici University<br>Bogazici University<br>Department of Chemical Engineering<br><br>Istanbul, 34342<br>Turkey<br>Attn: Bogazici University |
| Publisher Tax ID | GB 494 6272 12 |



Figure A.12. Copyrights of Figure 2.6 (page 2).

ELSEVIER LICENSE
TERMS AND CONDITIONS

Feb 24, 2021

This Agreement between Bogazici University -- Ceren Hatipoglu ("You") and Elsevier ("Elsevier") consists of your license details and the terms and conditions provided by Elsevier and Copyright Clearance Center.

| | |
|---|---|
| License Number | 5015181015222 |
| License date | Feb 24, 2021 |
| Licensed Content Publisher | Elsevier |
| Licensed Content Publication | Chemical Engineering Journal |
| Licensed Content Title | Intensified dimethyl ether production from synthesis gas with CO2 |
| Licensed Content Author | N. Furkan Ozturk,Ahmet K. Avci |
| Licensed Content Date | Aug 15, 2019 |
| Licensed Content Volume | 370 |
| Licensed Content Issue | n/a |
| Licensed Content Pages | 12 |
| Start Page | 885 |



Figure A.13. Copyrights of Figure 3.2 (page 1).

| | |
|---|---|
| End Page | 896 |
| Type of Use | reuse in a thesis/dissertation |
| Portion | figures/tables/illustrations |
| Number of figures/tables/illustrations | 1 |
| Format | both print and electronic |
| Are you the author of this Elsevier article? | No |
| Will you be translating? | No |
| Title | MULTIPLE ADIABATIC BEDS FOR EFFICIENT CONVERSION OF CO2-CONTAINING SYNGAS TO DIMETHYL ETHER |
| Institution name | Bogazici University |
| Expected presentation date | Feb 2021 |
| Portions | Fig. 1 |
| Requestor Location | Bogazici University<br>Bogazici University<br>Department of Chemical Engineering<br><br>Istanbul, 34342<br>Turkey<br>Attn: Bogazici University |
| Publisher Tax ID | GB 494 6272 12 |



Figure A.14. Copyrights of Figure 3.2 (page 2).